Regulation of potassium uptake in Caulobacter crescentus

Quintero Yanes, Alex Armando; Leger, Loic; Collignon, Madeline; Mignon, Julien; Mayard, Aurelie; Michaux, Catherine; Hallez, Regis

Published in:
Journal of Bacteriology

DOI:
10.1128/jb.00107-24

Publication date:
2024

Document Version
Version created as part of publication process; publisher's layout; not normally made publicly available

Journal of Bacteriology

Editor's Pick | Bacteriology | Full-Length Text

Regulation of potassium uptake in *Caulobacter crescentus*

Alex Quintero-Yanes,[1] Loïc Léger,[1] Madeline Collignon,[1] Julien Mignon,[2] Aurélie Mayard,[1] Catherine Michaux,[2] Régis Hallez[1,3]

AUTHOR AFFILIATIONS See affiliation list on p. 21.

ABSTRACT Potassium (K^+) is an essential physiological element determining membrane potential, intracellular pH, osmotic/turgor pressure, and protein synthesis in cells. Here, we describe the regulation of potassium uptake systems in the oligotrophic α-proteobacterium *Caulobacter crescentus* known as a model for asymmetric cell division. We show that *C. crescentus* can grow in concentrations from the micromolar to the millimolar range by mainly using two K^+ transporters to maintain potassium homeostasis, the low-affinity Kup and the high-affinity Kdp uptake systems. When K^+ is not limiting, we found that the *kup* gene is essential while *kdp* inactivation does not impact the growth. In contrast, *kdp* becomes critical but not essential and *kup* dispensable for growth in K^+-limited environments. However, in the absence of *kdp*, mutations in *kup* were selected to improve growth in K^+-depleted conditions, likely by increasing the affinity of Kup for K^+. In addition, mutations in the KdpDE two-component system, which regulates *kdpABCDE* expression, suggest that the inner membrane sensor regulatory component KdpD mainly works as a phosphatase to limit the growth when cells reach late exponential phase. Our data therefore suggest that KdpE is phosphorylated by another non-cognate histidine kinase. On top of this, we determined the KdpE-dependent and independent K^+ transcriptome. Together, our work illustrates how an oligotrophic bacterium responds to fluctuation in K^+ availability.

IMPORTANCE Potassium (K^+) is a key metal ion involved in many essential cellular processes. Here, we show that the oligotroph *Caulobacter crescentus* can support growth at micromolar concentrations of K^+ by mainly using two K^+ uptake systems, the low-affinity Kup and the high-affinity Kdp. Using genome-wide approaches, we also determined the entire set of genes required for *C. crescentus* to survive at low K^+ concentration as well as the full K^+-dependent regulon. Finally, we found that the transcriptional regulation mediated by the KdpDE two-component system is unconventional since unlike *Escherichia coli*, the inner membrane sensor regulatory component KdpD seems to work rather as a phosphatase on the phosphorylated response regulator KdpE~P.

KEYWORDS potassium transport, two-component system, Kup, KdpE, KdpD

Potassium (K^+) is the most abundant monovalent cation within living cells (1, 2) and it is essential to set the membrane potential and intracellular pH (2–5). As K^+ also emerges as an important regulator of bacterial physiology in view of its role in diverse processes (6–17) including biofilm formation, chemotaxis, cell to cell communication, or virulence, it is therefore expected that K^+ transport is tightly regulated. In many bacteria, the KdpDE two-component system (TCS) responds to potassium depletion by regulating the expression of the cognate high-affinity K^+ transporter KdpFABC (18). This inner membrane complex consists of four subunits, all encoded in the same operon, often together with the *kdpDE* genes (19, 20). In *Escherichia coli*, KdpD is a bifunctional inner membrane histidine kinase—harboring both kinase and phosphatase activities—with four transmembrane domains separating two N-terminal cytoplasmic input domains

Editor Anke Becker, Philipps-Universitat Marburg Fachbereich Biologie, Marburg, Germany

Address correspondence to Régis Hallez, regis.hallez@unamur.be.

The authors declare no conflict of interest.

See the funding table on p. 21.

Received 9 March 2024
Accepted 13 July 2024

(called KdpD and Usp) and three C-terminal cytoplasmic domains (GAF, HisKA, and HATPase_C). While the two last domains are obviously required for the autophosphorylation of KdpD, the GAF domain might be responsible for sensing intracellular K^+ (21) whereas extracellular K^+ might be sensed by the transmembrane domains (22). Based on these data, KdpD was proposed to act as a dual sensor for K^+, able to sense both extracellular and intracellular K^+. Whereas the extracellular K^+ was shown to inhibit KdpD kinase activity, its phosphatase activity was stimulated by intracellular K^+ (23). Several proteins have been found to interact with KdpD, such as the universal stress protein UspC identified as a scaffolding protein that interacts with the N-terminal Usp domain. It has been proposed that UspC binding enhances KdpE phosphorylation by KdpD at high K^+ concentration at which KdpE would not be phosphorylated (24). The unphosphorylated form of $EIIA^{Ntr}$, which belongs to the PTS^{Ntr}, interacts with the catalytic domain KdpD to activate its autokinase activity (25, 26). K^+ availability ultimately determines the phosphorylation status of the response regulator KdpE and thus provides a tight regulation of *kdpFABC* expression as well as a robust homeostasis in fluctuating environments (23).

Other K^+ transporters have been described in detail in Gram-negative bacteria, such as the inner membrane low-affinity Trk and Kup systems for uptake, and the KefB efflux pump. The Trk potassium uptake system is highly conserved in bacteria and works as a multi-subunit complex comprising the TrkG/H, TrkA, and TrkE proteins. TrkH, and the extra copy known as TrkG in *E. coli*, are transmembrane transporter units, which interact with the peripheral protein TrkA and the ATP-binding protein TrkE in the cytoplasmic leaflet to control extracellular potassium uptake when high extracellular concentrations of K^+ are available (27–29). Kup is a single protein, constitutively expressed and thought to function as K^+/Na^+ symporter (28, 30, 31).

Recently, it was reported that glutathione controls cell division via negative regulation of KefB in the Gram-negative oligotrophic α-proteobacterium *Caulobacter crescentus* (32). Indeed, mutants unable to synthesize glutathione led to cell filamentation and decreased intracellular K^+ levels. Interestingly, these phenotypes were suppressed by mutations in the KefB efflux pump, suggesting that low intracellular K^+ concentration was responsible for the cell division defect. *C. crescentus* has been extensively used as a model for cell cycle studies since it divides asymmetrically to give birth to a larger sessile stalked cell and a smaller flagellated swarmer cell (33). DNA replication and cell division take place only in sessile stalked cells, whereas the swarmer cells remain in a non-replicative but chemotactically active and motile phase able to explore new environments. Once swarmer cells find a suitable—resourceful—habitat for reproduction, they differentiate into stalked cells and concomitantly start DNA replication. In contrast, upon deprivation of environmental resources, the swarmer cells do not differentiate into replicative stalked cells (34).

In this study, we characterized the response of *Caulobacter* cells grown in environments containing what we defined as limiting, abundant, and excessive K^+ concentrations. *In silico* analyses revealed that *C. crescentus* does not have Trk system components but encodes a putative transporter with a cytoplasmic TrkA-like domain. Moreover, in addition to the KefB and KefC efflux pumps, we found genes predicted to code for Kup and KdpABC transporters as well as a KdpDE TCS. We generated mutants of these predicted K^+ transporters and assessed their fitness in limiting, abundant, and excessive K^+ environments. We also characterized the KdpDE system and determined its regulon by RNA-seq.

RESULTS

Growth of *C. crescentus* at different K^+ concentrations

To primarily assess the impact of K^+ on *C. crescentus* fitness, the wild-type (WT) strain was grown in K^+-free minimal medium (M2G-K) supplemented with K^+ at different concentrations using either KCl or a combination of K_2HPO_4 and KH_2PO_4 (K_2HPO_4 + KH_2PO_4) like the one used in standard M2G minimal medium (Fig. 1). First, when phosphate salts

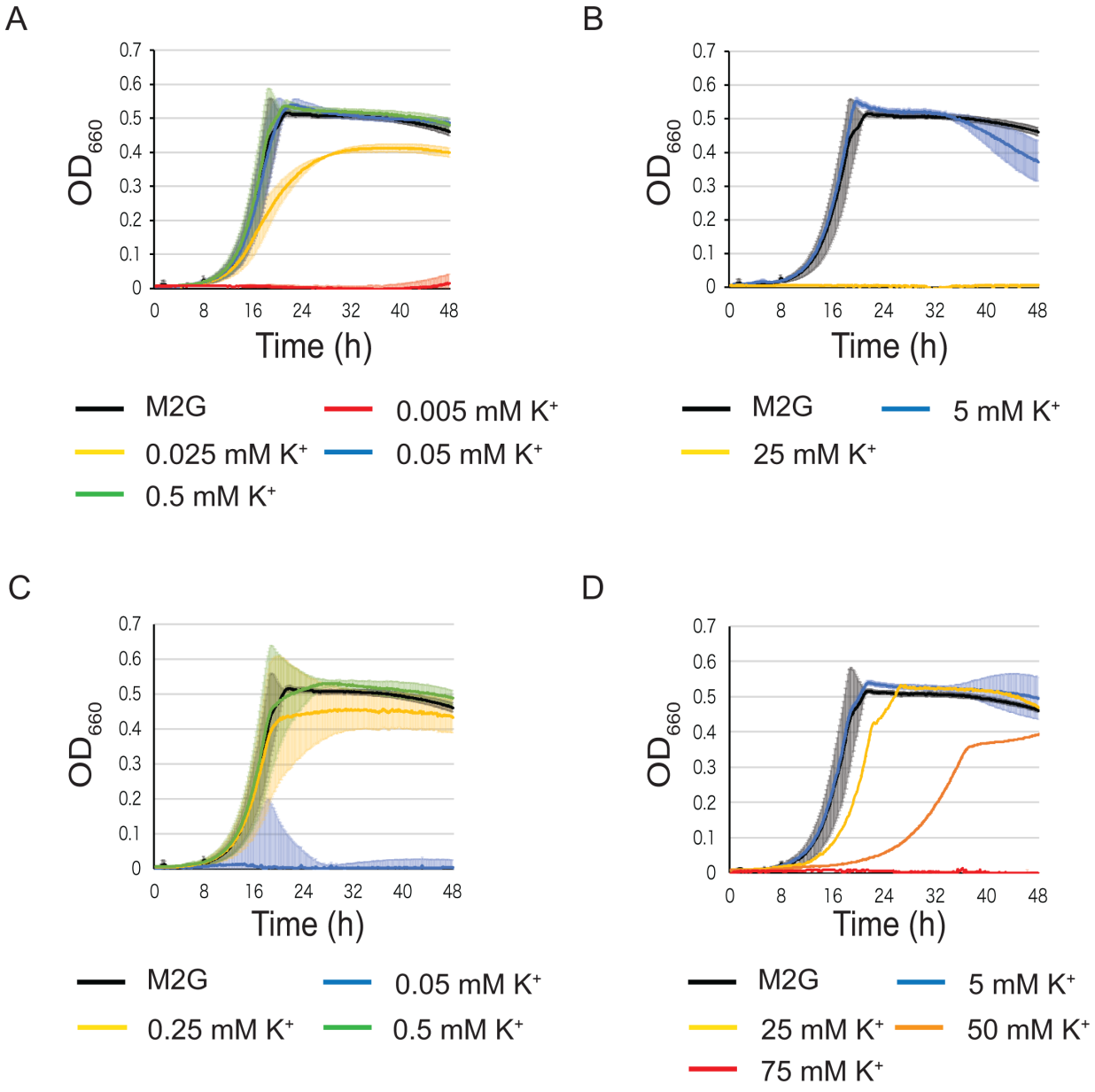

FIG 1 Impact of K^+ on *C. crescentus* growth. Growth of WT in M2G-K supplemented with different K^+ concentrations using K_2HPO_4 + KH_2PO_4 (A, B) and KCl (C, D) as K^+ source. Data represent average, *n* = 3, and error bars = ±SD. Other concentrations tested are presented in Fig. S1.

were used as K^+ source, we observed that compared to M2G, which contains 7 mM K^+, growth started to be significantly impaired at concentrations below or equal to 0.025 mM and above or equal to 7 mM (Fig. 1A and B). Second, by using KCl, we found different K^+ concentrations critical for growth since the WT already failed to grow at 0.05 mM but supports growth up to 25 mM (Fig. 1C and D; Fig. S1A). Notwithstanding these differences likely due to the $PO4^{3-}$ and Cl^- counter-anions, the growth of the WT at K^+ concentrations ranging from 0.5 mM to 5 mM was indistinguishable from the one in M2G, that is 7 mM (Fig. 1). Therefore, based on these data, we will use in this study potassium phosphate salts at 0.025 mM and 0.5 mM, respectively, as limiting and abundant concentrations while KCl will be used at 50 mM as excessive concentration.

K^+ transport and regulation systems in *C. crescentus*

By using *in silico* analyses, we found in the genome of *C. crescentus* NA1000 (NC_011916.1) several genes encoding potential K^+ uptake [*kup* (*CCNA_00130*) and *kdpABCDE* (*CCNA_01663–1667*)] or efflux [*kefB* (*CCNA_00204*), *kefC* (*CCNA_03611*), and *kefG* (*CCNA_00205*)] systems. Although Trk orthologs were not found, a putative transporter (*CCNA_01688*) containing a cytoplasmic TrkA-like domain was identified. Based on the function of the Kdp, Kef, Kup, and Trk systems in other bacteria (2, 12, 35–37), we predicted that K^+ transport in *C. crescentus* might occur via CCNA_01688, KefBG, KefC, and Kup when potassium is abundant in the environment, whereas the Kdp system might be inactive (38, 39). In contrast, K^+-depleted conditions should activate the KdpDE TCS and trigger expression of the high-affinity KdpABC transporter (40).

To test these predictions, we first constructed knock-out (KO) mutants for all the K^+ transport and regulatory systems described above. We successfully inactivated all these genes except *kup*, suggesting it might be essential at least at the K^+ concentration found in the complex medium peptone yeast extract (PYE) used to construct the KO strains. Note that Δ*kefB* and Δ*kdpABCDE* (hereafter referred to as Δ*kdp*) were respectively used as *kefBG* and *kdp* inactive mutants. Then, we measured the growth for the mutants at different K^+ concentrations (Fig. 2). In limiting (0.025 mM) K^+ conditions, only Δ*kdp* had a strong growth delay but could still grow (Fig. 2A), suggesting that another transporter is used in K^+ depletion conditions, at least when *kdp* is inactive. All the KO mutants grew equally well as the WT in minimal medium supplemented with abundant (0.5 mM) K^+ concentration (Fig. 2B) or in complex medium (Fig. S1B). At excessive (50 mM) K^+ concentration, we found that (i) Δ*CCNA_01688* had a slight growth delay; (ii) Δ*kdp* had a lower plateau; and (iii) Δ*kefC* barely grew in comparison to WT (Fig. 2C). Interestingly, the growth delay of Δ*CCNA_01688* and the lower plateau of Δ*kdp* were not observed in complex PYE medium supplemented with an excess of K^+ whereas Δ*kefC*, like in minimal medium, did not grow in these conditions (Fig. S1C).

K^+-dependent essential genome

Transposon mutagenesis coupled to next-generation sequencing (Tn-seq) was used to determine the core set of genes important for adaptation and response to abundant or limiting K^+ condition (Fig. 3A). We used M2G-K with 1% agar concentration to lower as much as possible K^+ traces from the agar in our experiment. Indeed, even at 1% agar, the K^+ traces were sufficient to allow WT cells to grow without exogenous source of K^+ (on M2G-K, Fig. 3B). In contrast, at least 0.025 mM K^+ had to be supplemented to M2G-K to allow growth of Δ*kdp*, while at 0.5 mM K^+, both the mutant and the WT grew similarly

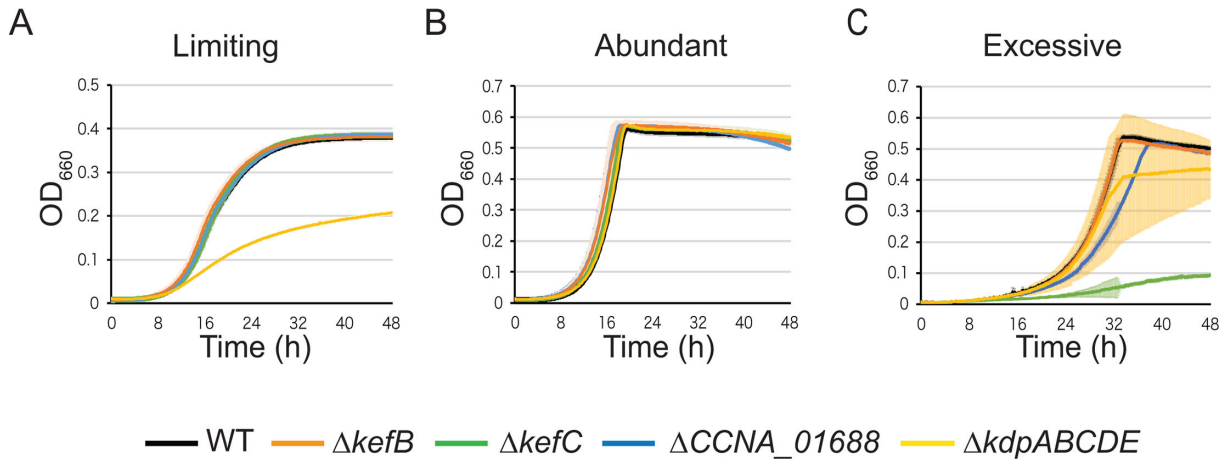

FIG 2 Deletion of K^+-related genes impact *C. crescentus* growth. Growth of WT, Δ*kefB*, Δ*kefC*, Δ*CCNA_01688*, and Δ*kdpABCDE* mutants in minimal medium M2G-K supplemented with (A) limiting (0.025 mM), (B) abundant (0.5 mM), and (C) excessive (50 mM) K^+ concentrations. Data represent average, $n = 3$, and error bars = ±SD.

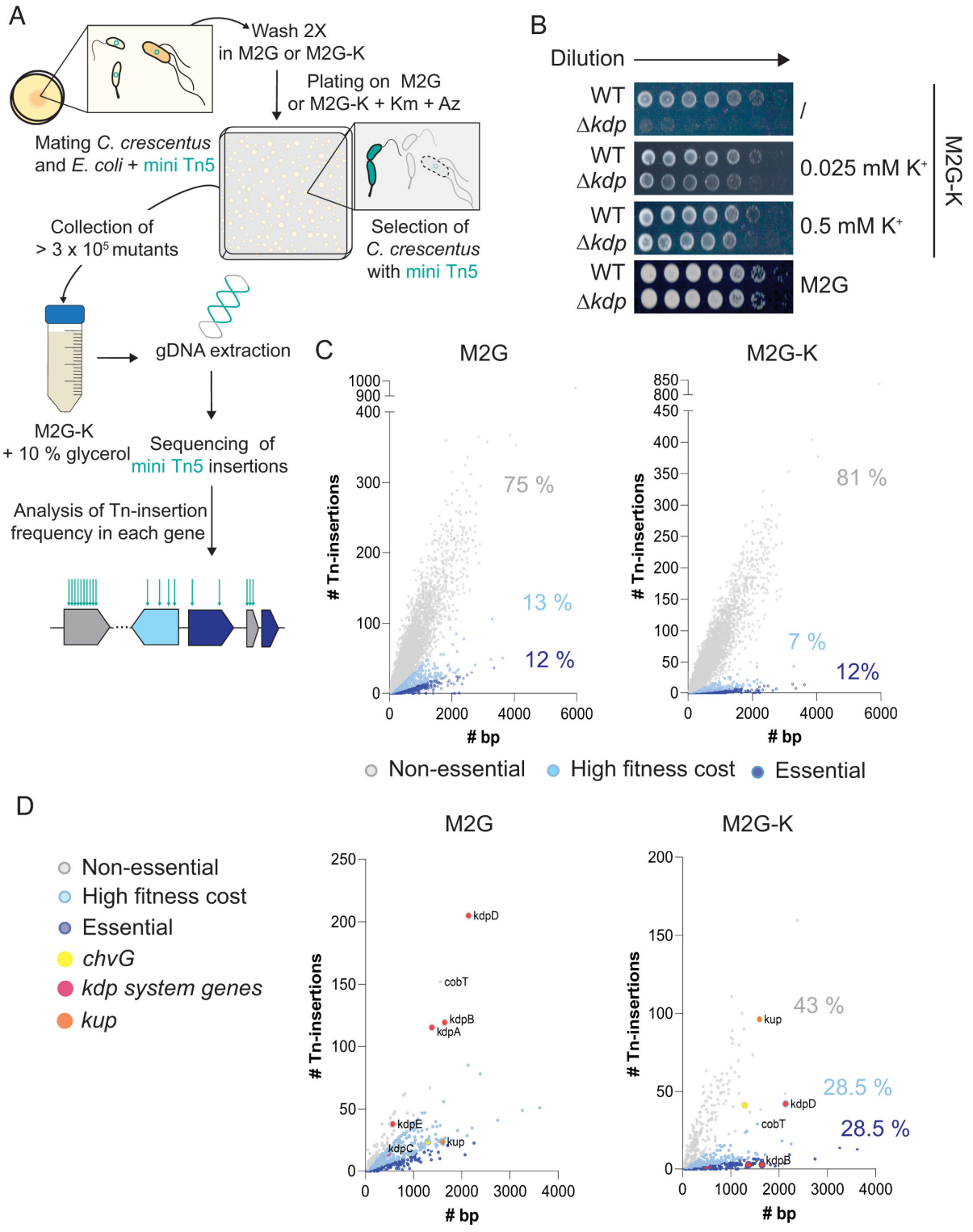

FIG 3 Tn-seq profile of *C. crescentus* cells in limiting K^+ conditions. (A) Diagram of the Tn-seq experiment. As explained in detail in Materials and Methods section, *E. coli* cells were used to deliver a mini Tn5 vector into *C. crescentus* by conjugation. Mating spots were washed twice in either M2G or M2G-K. Cells were plated in either M2G or M2G-K square plates supplemented with kanamycin (Km) and aztreonam (Az) to counter select *C. crescentus* cells with Tn5 insertions (green cells) over *C. crescentus* without insertions and *E. coli* cells. Cells were collected to complete >3 × 10^5 clones. Thereafter, gDNA extraction and Tn5-directed sequencing were performed to determine the frequency of insertions for each gene in *C. crescentus* genome and determine genes that are essential, high fitness cost, or non-essential in M2G and M2G-K plates. (B) Growth of WT and Δ*kdp* cells in M2G-K plates without or supplemented with K^+. (C) Number of Transposon insertions

(Continued on next page)

FIG 3 (Continued)

(#Tn insertions) against the length (#bp) of 4,186 genes in M2G and M2G-K media. Non-essential genes are highlighted in gray, high fitness cost genes in light blue, and essential in dark blue. (D) Representation of genes that changed in their fitness cost categories according to analysis done in M2G and M2G-K (C). (C, D) The percentage of genes in each category is indicated following the color code.

(Fig. 3B). Therefore, we decided to use M2G-K without exogenous K^+ and M2G plates, respectively, as the limiting and abundant K^+ conditions for the Tn-seq (Fig. 3B).

We analyzed the frequency of Tn insertions and observed a bimodal distribution that allowed us to visualize two clusters of genes in each condition, one with low density of Tn insertions (considered as essential genes) and the other one with a higher density (considered as non-essential genes) (Fig. S2A). Based on this frequency of Tn insertions, we used Ward's clustering analysis (41) and defined three fitness cost categories, which are (i) essential, (ii) High Fitness Cost (HFC), and (iii) non-essential. Among the 4,186 annotated genes in *C. crescentus*, the percentage of essential genes in both media (M2G and M2G-K) was similar (~12%), while the percentage of HFC genes was lower (~7%) in M2G-K than in M2G (~13%). Hence, the percentage of non-essential genes was higher in M2G-K (~81%) than in M2G-K (~75%) (Fig. 3C; Table S2). The shift from the HFC to the non-essential category in *C. crescentus* cells grown in M2G-K could be explained by the reduction of osmotic stress in this medium. Indeed, we showed recently that M2G generates a cell envelope stress for *C. crescentus* due to the high content of monovalent cations (42).

Genes with known or predicted biological functions were grouped according to the classification of cluster of orthologs groups (COG) (Fig. S2B). This allowed to highlight biological functions that are enriched in abundant and limited K^+ conditions. Overall, the COG enrichment in the three fitness categories (essential, HFC, and non-essential) was substantially similar in both M2G and M2G-K media. The C group "energy production and conversion" genes was the most abundant for all the fitness categories in M2G-K, as well as for essential and non-essential genes in M2G, while for HFC genes, it was the second most abundant, after the J group "translation, ribosomal structure and biogenesis."

By comparing the gene pool in each category for each medium, we identified a set of 537 genes that changed their fitness cost from M2G to M2G-K and vice versa (Fig. 3D; Table S2), including 153 genes which became exclusively essential (28.5%), 153 HFC (28.5%), and 231 non-essential (43%) in M2G-K. First, we observed that the TCS genes *chvGI*, known to be HFC in M2G due to its response to hyperosmotic stress (42), became non-essential in M2G-K, thereby supporting that M2G-K is a hypo-osmotic environment compared to M2G. Second, all the *kdp* genes categorized as non-essential in M2G became essential in M2G-K, except *kdpD* which became HFC. In contrast, *kup* moved from the HFC category in M2G to non-essential one in M2G-K. This confirms the importance of the Kdp and Kup systems, respectively, in limiting and abundant K^+ conditions. Considering the conservation of the *kdp* system in bacteria, it is intriguing that *kdpD*—encoding the histidine kinase component—did not have the same fitness cost in M2G-K than the genes coding for the transporter (*kdpABC*) and the response regulator (*kdpE*) components. While this supports that KdpE likely regulates, directly, the expression of *kdpABC* genes, it suggests that KdpD and KdpE have different regulatory effects on growth in K^+-depleted environments. Finally, we did not observe changes in fitness for the other predicted potassium transport systems since all of them were categorized as non-essential genes in both M2G and M2G-K, further supporting that CCNA_01688, KefBG, and KefC are not important for growth in abundant and limiting K^+ conditions, although we cannot rule out some redundancy between these systems.

Kup becomes dispensable in limiting K^+ conditions

The Tn-seq data suggest that inactivation of *kup* gene could be facilitated at limiting K^+ concentrations (Fig. 3D; Table S2). Kup has been described in different bacteria as the major K^+ transporter, essential in hyperosmotic conditions using sucrose as osmotic stressor (43, 44). Moreover, in a previous study, we found that the TCS ChvGI in *C.*

crescentus positively controls the expression of *kup* in hyperosmotic conditions (42). In agreement with this, we could not obtain a Δ*kup* strain by using a markerless recombination approach on complex medium (PYE) plates supplemented with 3% sucrose for the SacB-dependent counterselection. Since addition of sucrose considerably increases the osmolality of the media (45), we successfully generated a Δ*kup* mutant on a minimal medium lacking both Na_2HPO_4 and KH_2PO_4 salts and supplemented with 0.5% sucrose. Interestingly, we observed that the Δ*kup* mutant grew in limiting K^+ concentration, although at a slower growth rate but to a higher plateau compared to the WT (Fig. 4A). As expected from the Tn-seq data, we found that Δ*kup* failed to grow when exposed to abundant and excessive K^+ concentrations (Fig. 4A). We also confirmed that *kup* is essential in hypertonic conditions since the mutant did not grow in limiting K^+ conditions when 3% sucrose were added. (Fig. 4A). Together, these data indicate that Kup allows potassium uptake in abundant and excessive K^+ conditions but can be detrimental for unknown reasons at limiting K^+ concentrations.

While characterizing the growth of Δ*kdp* cells on M2G-K plates (Fig. 3A), we inadvertently selected growth suppressors that improved the growth of Δ*kdp* in limiting K^+ conditions (Fig. S2D). Whole genome sequencing analyses of several of these suppressors allowed the identification of three mutations in *kup:* kup_{A87P}, kup_{G253S}, and kup_{S456R}. Using homologous recombination, we constructed these mutations in WT and Δ*kdp* backgrounds. First, these *kup* mutations did not have any significant fitness cost when K^+ was not limiting (Fig. 4B). Second, the single point mutants in an otherwise WT background grew similarly to the WT strain at limiting K^+ concentrations (Fig. 4B). Third, each *kup* mutation suppressed the defect of Δ*kdp* when grown in limiting K^+ condition, although to a lesser extent for kup_{S456R} than for the two other suppressor mutations (Fig. 4B).

To get molecular insight into the mutation-mediated improved K^+ binding/transport by Kup, molecular dynamics (MD) simulations were carried out on the modeled WT Kup protein and each of the three mutants (A87P, G253S, and S456R) in an environment mimicking the lipid composition of *Caulobacter* inner membrane (46, 47) (Fig. S3A). Then, Kup coordinates were aligned to one protomer of *Bacillus subtilis* KimA (PDB entry: 6S3K), the only available Cryo-Electron Microscopy (Cryo-EM) structure of a KUP family protein (48) (Fig. 5A). This Cryo-EM structure corresponds an "inward-occluded" state with two K^+ cations trapped inside KimA. The eight residues in KimA described to be involved in the coordination and transport of these two K^+ cations are conserved in Kup with the following correspondences (KimA/Kup): D36/D54, Y43/Y61, D117/D146, T121/T150, S125/S154, T230/T260, E233/E263, and Y377/Y410.

The A87P mutation leads to only a few changes, the WT conformation being mainly retained, but a flipping of E263 toward the orientation described for the corresponding glutamate in KimA (E233) is observed (Fig. 5B). The same observation was made with the G253S and S456R mutations (Fig. 5C and D), suggesting that E263 reversal is structurally relevant for the increase of K^+ transport by the Kup mutants. Furthermore, although to a lesser extent, the position of another residue is also changed in the three mutants. Indeed, D146 points more toward the K^+ binding cavity, making the carboxylate group more available for coordination (Fig. 5B through D). Finally, G253S and S456R mutants are characterized by a reorientation of both Y61 and Y410 to a position close to that of Y43 and Y377, respectively, in KimA, with the tyrosyl moiety directed toward the putative K^+ location (Fig. 5C and D). Thus, our MD simulations suggest that despite their different locations on Kup, the three mutations lead to subtle structural changes in the orientation of key residues described to directly participate in the binding and/or transport of K^+. The reorientation of these residues might facilitate binding of K^+ cations at lower concentration.

Altogether, these data indicate that (i) Kup allows potassium uptake in abundant and excessive K^+ conditions, and that (ii) mutations in Kup improve K^+ transport at limiting concentrations, likely by increasing affinity for K^+.

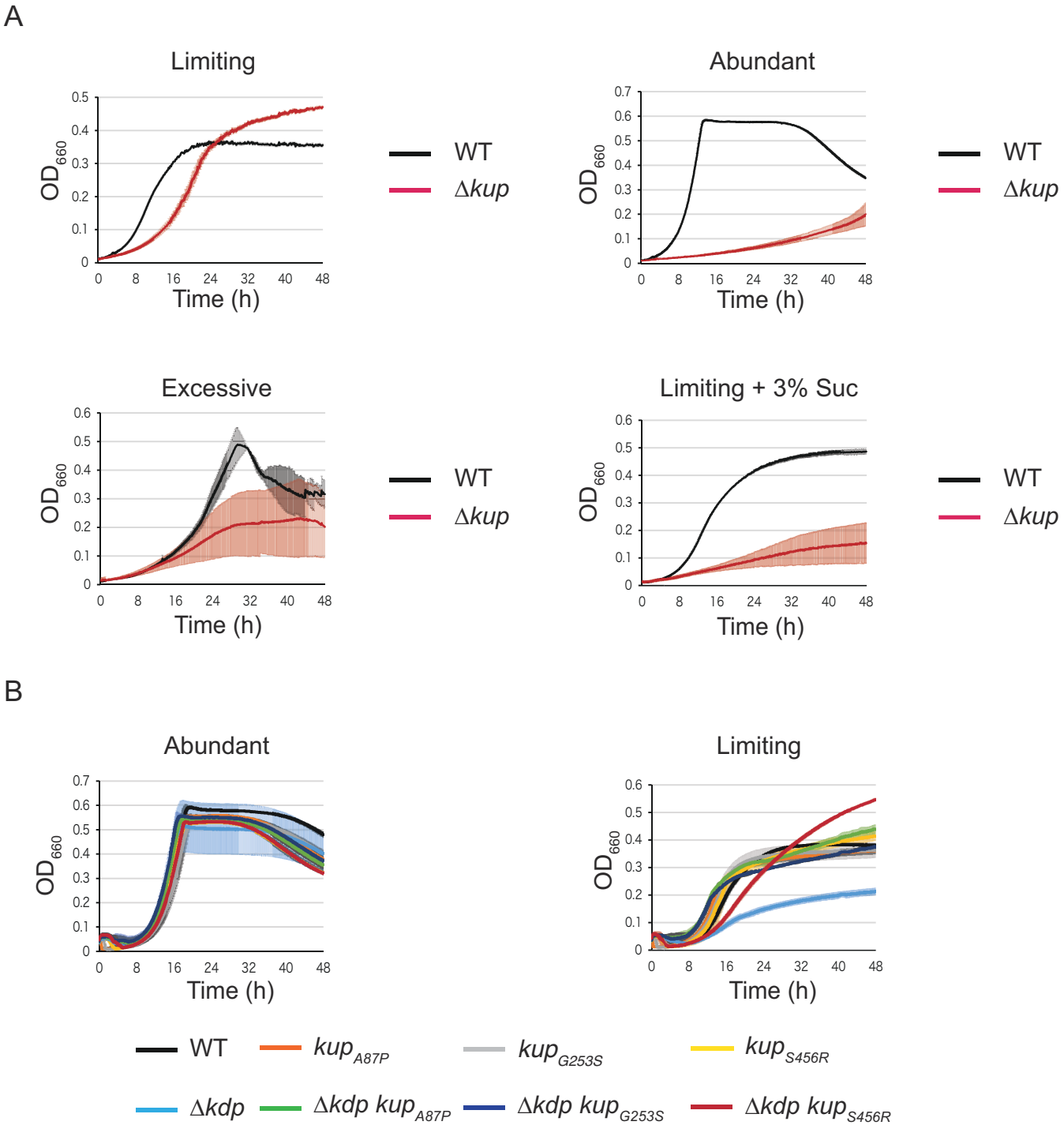

FIG 4 Impact of deletion and overexpression of the *kup* gene. (A) Growth of WT and Δ*kup* mutant in minimal medium M2G-K supplemented with limiting (0.025 mM), abundant (0.5 mM), excessive (50 mM) K^+ concentrations or limiting (0.025 mM) K^+ concentrations and 3% sucrose. (B) Growth of WT, kup_{A87P}, kup_{G253S}, and kup_{S456R} in an otherwise WT or Δ*kdp* background, in abundant and limiting K^+ conditions. Data represent average, $n = 3$, and error bars = ±SD.

K^+- and KdpE-dependent regulons

To further characterize the response of *C. crescentus* to K^+-depleted conditions, we performed RNA-seq on RNA samples extracted from cells grown in minimal medium in K^+-limiting or -abundant conditions. In our experiment, we identified a total of 594 genes —385 upregulated and 209 downregulated—whose expression was impacted upon

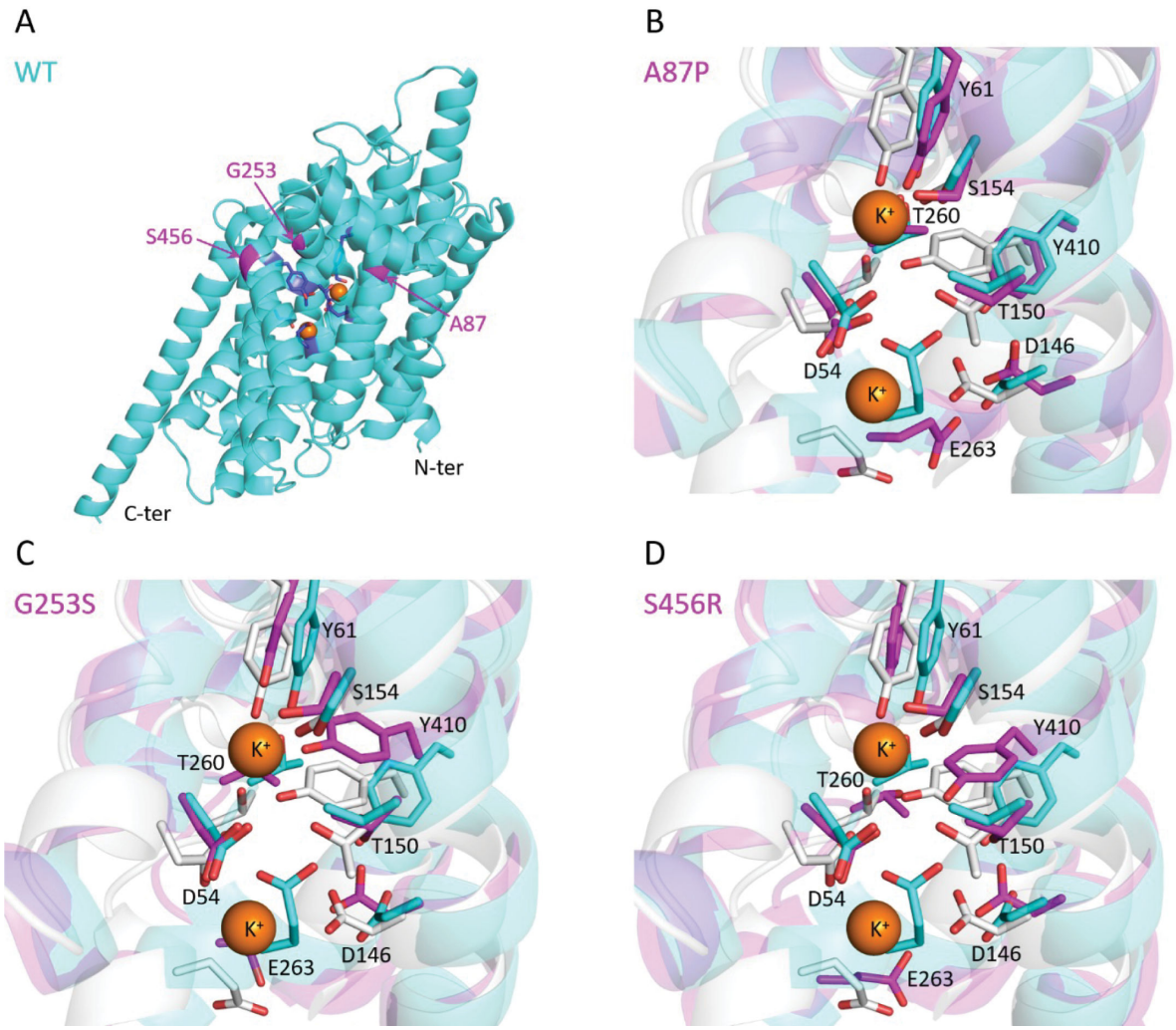

FIG 5 Molecular dynamics-highlighted structural changes of the putative K^+ binding sites of Kup mutants. (A) Snapshot of Kup WT after 1 µs of simulation. The protein is represented in cyan as cartoon, the considered mutation sites are colored in magenta and indicated by arrows, and the residues composing the KimA-based K^+ binding cavity are highlighted as sticks in dark blue. (B) Snapshot of the KimA-based K^+ binding site of Kup_{A87P}, (C) Kup_{G253S}, and (D) Kup_{S456R} after 1 µs of simulation. On each of these panels, WT Kup (cyan) and mutated Kup (magenta) aligned to KimA (PDB entry: 6S3K; light gray) are shown as cartoon, conserved residues between Kup and KimA constitutive of the K^+ binding pocket are represented as sticks in the corresponding color, and K^+ cations as orange spheres. The displayed amino acid numbering only corresponds to Kup sequence.

K^+ limitation with at least a two-fold change (FC ≥2) and a false-discovery rate (FDR) lower than 5% (P_{adj} ≤0.05) (Fig. 6A). As expected, this experiment confirmed that the expression of *kdp* genes was strongly induced in the K^+-depleted medium. Among the other upregulated genes, we found genes coding for the phosphate starvation protein PhoH (*CCNA_02727*), a xylose isomerase family protein (*CCNA_01701*), a TonB-dependent receptor (TBDR, *CCNA_01859*), an AraC family transcription regulator (*CCNA_01858*), and hypothetical proteins (*CCNA_03313* and *CCNA_03970*) (Fig. 6A; Table S3). Among the top downregulated candidates, we found genes expressing a small RNA (*CCNA_R0158*), a hemin receptor (*CCNA_02277*), a putative transporter (*CCNA_03022*), a protein with a calcium binding EF Hand binding domain (*CCNA_02274*) and the chaperones GroES (*CCNA_00722*) and GroEL (*CCNA_00721*) (Fig. 6A; Table S3).

As our results suggest that the Kdp system is important for growth upon K^+ depletion, we also performed RNA-seq experiments with a Δ*kdpE* mutant grown in limiting K^+ concentrations. Then, we compared the RNA enrichment in Δ*kdpE* vs WT to determine

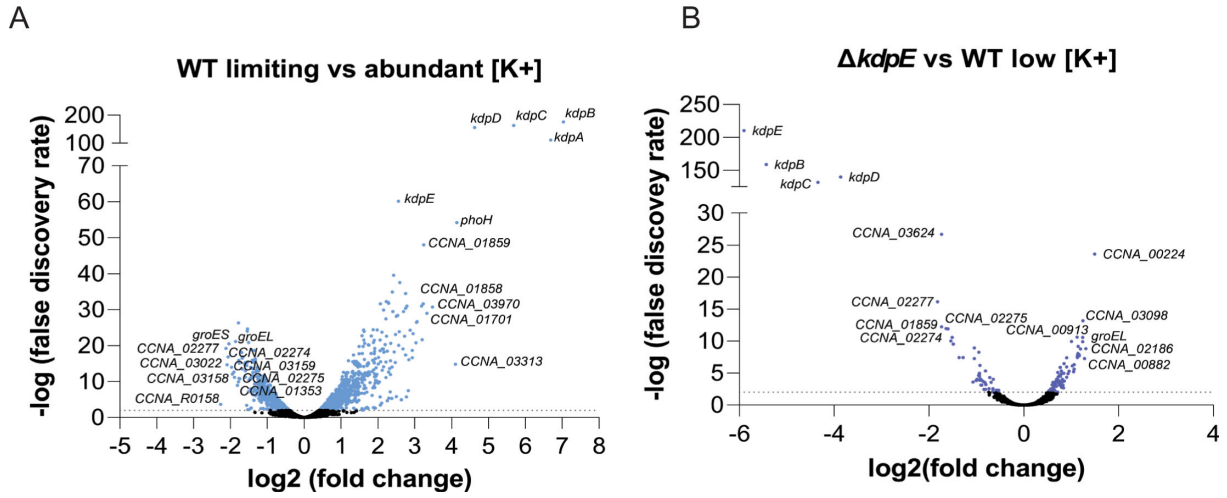

FIG 6 K^+- and KdpE-dependent regulon. (A, B) Volcano plots representing the relation between the $\log_2$ FC and −log FDR on gene expression between (A) WT in limiting vs abundant K^+ condition, and (B) Δ*kdpE* vs WT in limiting K^+ condition. Genes identified are presented as dots. Significant downregulated and upregulated genes are presented as blue (A) and purple (B) dots, while genes with no significant alterations are presented as black dots. Top 10 downregulated and upregulated genes are highlighted for each analysis.

which genes are affected by KdpE in a K^+-depleted condition using the same parameters, FC ≥2 and $P_{adj} \leq 0.05$. Compared to WT, we found 20 upregulated and 19 downregulated genes in Δ*kdpE* grown in the K^+-depleted medium (Fig. 6B; Table S4). Among the 19 downregulated genes in Δ*kdpE* (Table S4), 95% (18/19) were also found in the regulon of the WT starved for K^+, 11 upregulated (including *kdp* genes; Table S3) and 7 downregulated (Table S3). This suggests that KdpE is strictly required to activate the expression of the 11 genes in a K^+-depleted environment. On the contrary, the seven other genes that are repressed in WT cells upon K^+ depletion are even further downregulated in the absence of KdpE, suggesting that KdpE limits the repression of these genes. The expression of the last gene (*CCNA_00930*) was insensitive to K^+ concentration while downregulated in Δ*kdpE* (Table S4), suggesting that this gene is positively regulated by KdpE but independently of the K^+ concentration. Among the 20 upregulated genes in Δ*kdpE* (Table S4), only 35% (7/20) were also found in the regulon of the WT starved for K^+, two downregulated (*groEL* and *groES*; Table S3) and five upregulated (Table S3). This indicates KdpE is required to repress *groEL* and *groES* upon K^+ depletion while it limits the activation of the five other genes in a K^+-depleted environment. The remaining 13 upregulated genes in Δ*kdpE* (Table S4) were insensitive to K^+ availability, suggesting that they are likely repressed by KdpE but in a K^+-independent way.

Surprisingly, the vast majority (555 genes; 92.8%) of the 594 genes whose expression changed in the WT grown in K^+-limiting conditions seems to be KdpE-independent, suggesting that other regulators, yet to be discovered, are activated upon K^+ depletion. An alternative explanation might be that Δ*kdpE* cells exposed to limiting K^+ concentration suffer from a general stress response, which ultimately leads to global transcriptional changes. This could also explain why more than a third of the 39 genes (14/39) found in the Δ*kdpE* regulon were not identified in the K^+ regulon.

In order to unveil genes whose expression is directly regulated by KdpE, we identified the DNA regions bound by KdpE using ChIP-seq in WT and Δ*kdpE* cells grown either at abundant or limiting K^+ concentrations. The highest number of reads were found in the *kdp* promoter (P_{kdp}) only in the WT grown at low K^+ concentrations. Interestingly, this peak was absent in WT grown in abundant K^+ conditions as well as in Δ*kdpE* both at high and low K^+ concentrations, suggesting KdpE binds to the P_{kdp} only when *C. crescentus* is starved for K^+, that is likely when KdpE is phosphorylated and abundant. While several other peaks were identified in this condition, these peaks were also present in the Δ*kdpE*, suggesting that they correspond to unspecific peaks recognized by the

polyclonal antibodies. Indeed, while the KdpE protein was only detected in WT cells, at a higher level in limiting than in abundant K^+ conditions, several proteins other than KdpE were detected in Δ*kdpE* cells (Fig. S4A). Although we do not rule out the possibility that KdpE binds directly several promoter regions in *C. crescentus*, the only confident target identified in our ChIP-seq is P_{kdp}. We also conducted ChIP-seq in strains in which *kdpE* was expressed under the xylose inducible promoter (P_{xylX}::*kdpE*) in a Δ*xylX* Δ*kdpE* or Δ*xylX* Δ*kdpDE* background. Expression of *kdpE* from P_{xylX} efficiently complemented the growth of both strains in the presence of xylose since Δ*xylX* Δ*kdpE* P_{xylX}::*kdpE* cells grew similarly to Δ*xylX* or WT cells whereas Δ*xylX* Δ*kdpDE* P_{xylX}::*kdpE* cells grew at a higher plateau (Fig. S4B) like Δ*kdpD* cells (see below). Moreover, KdpE was easily detected by western blot in both strains, although KdpE protein levels were lower in Δ*kdpDE* than in Δ*kdpE* (Fig. S4C). Surprisingly, the peak at P_{kdp} was higher in the Δ*kdpDE* background than in the Δ*kdpE* one (Fig. S4D), suggesting that KdpE could be more active (hyperphosphorylated) in the absence of KdpD and therefore that KdpD mainly acts as a negative regulator of KdpE~P.

C. crescentus KdpD regulates KdpE both positively and negatively

To further assess the role of the *C. crescentus* Kdp system in K^+-limiting conditions, we first constructed KO mutants of the transport complex (Δ*kdpABC*) and the TCS (Δ*kdpDE*) genes. In comparison to the WT, both Δ*kdpABC* and Δ*kdpDE* mutants had a growth delay at limiting but not at abundant K^+ concentration (Fig. 7A; Fig. S5A). Moreover, both mutants grew similarly, suggesting that the *kdpABC* is not expressed in the absence of the TCS, as described in other bacteria.

To study the histidine kinase (HK) *kdpD* and response regulator *kdpE* genes independently of each other, we constructed single KO mutants, Δ*kdpD* and Δ*kdpE*. Deletion of *kdpE* resulted in a similar growth delay than the ones displayed by Δ*kdpABC*, Δ*kdpDE*, and Δ*kdpABCDE* (Fig. 7A; Fig. S5B). On the contrary, Δ*kdpD* behaves differently since compared to WT, it had a slight but reproducible growth delay in exponential phase while it later reached a higher plateau in stationary phase (Fig. 7A). While the growth defects displayed by both single Δ*kdpD* and Δ*kdpE* mutants in limiting K^+ condition could be complemented (Fig. 7B and C), expressing back *kdpE* in Δ*kdpDE* cells led to the same growth behavior than the single Δ*kdpD* mutant, that is a slight growth delay in exponential phase and a higher plateau in stationary phase (Fig. 7C; Fig. S5C). In addition, the fact that Δ*kdpE* is epistatic on Δ*kdpD*, since Δ*kdpDE* grew as poor as Δ*kdpE* or Δ*kdpABC* (Fig. 7A), shows that KdpE is entirely responsible for the Δ*kdpD* phenotypes. Together, these data support that both components of the TCS are important for the growth in K^+-depleted environments and suggest that KdpD and KdpE have antagonistic roles for growth in such conditions.

To better understand the KdpDE regulatory mechanism, we constructed *kdpD* and *kdpE* catalytic point mutants (Fig. S5D) and assessed their impact on growth in abundant and limiting K^+ conditions. In agreement with what we observed with the KO mutants, all the catalytic mutants grew similarly to the WT in abundant K^+ conditions (Fig. S5E). At limiting K^+ concentrations, however, the phospho-ablative mutant of KdpE (*kdpE*$_{D56A}$) had a strong growth delay, similar to the one displayed by Δ*kdpE* (Fig. 7D; Fig. S5F). In contrast, the phospho-mimetic mutant (*kdpE*$_{D56E}$) grew similarly to the WT up to the late exponential phase, to finally reach a higher final OD comparable to the one observed with Δ*kdpD* grown in same conditions (Fig. 7D; Fig. S5F). Both the WT KdpE and $KdpE_{D56A}$ proteins were detected at a low but similar level when K^+ concentration was not limiting, such as in complex PYE medium. On the contrary, the level of the $KdpE_{D56E}$ was much higher in these conditions, likely because it constitutively stimulates the expression of the *kdpABCDE* operon (Fig. S4A). In contrast, in limiting K^+ conditions, WT KdpE reached high levels, similar to $KdpE_{D56E}$, whereas $KdpE_{D56A}$ levels did not increase, likely because $KdpE_{D56A}$ cannot be phosphorylated. Together, these data support that *kdpE*$_{D56A}$ and *kdpE*$_{D56E}$ behave, respectively, as phospho-ablative and phospho-mimetic mutants of KdpE.

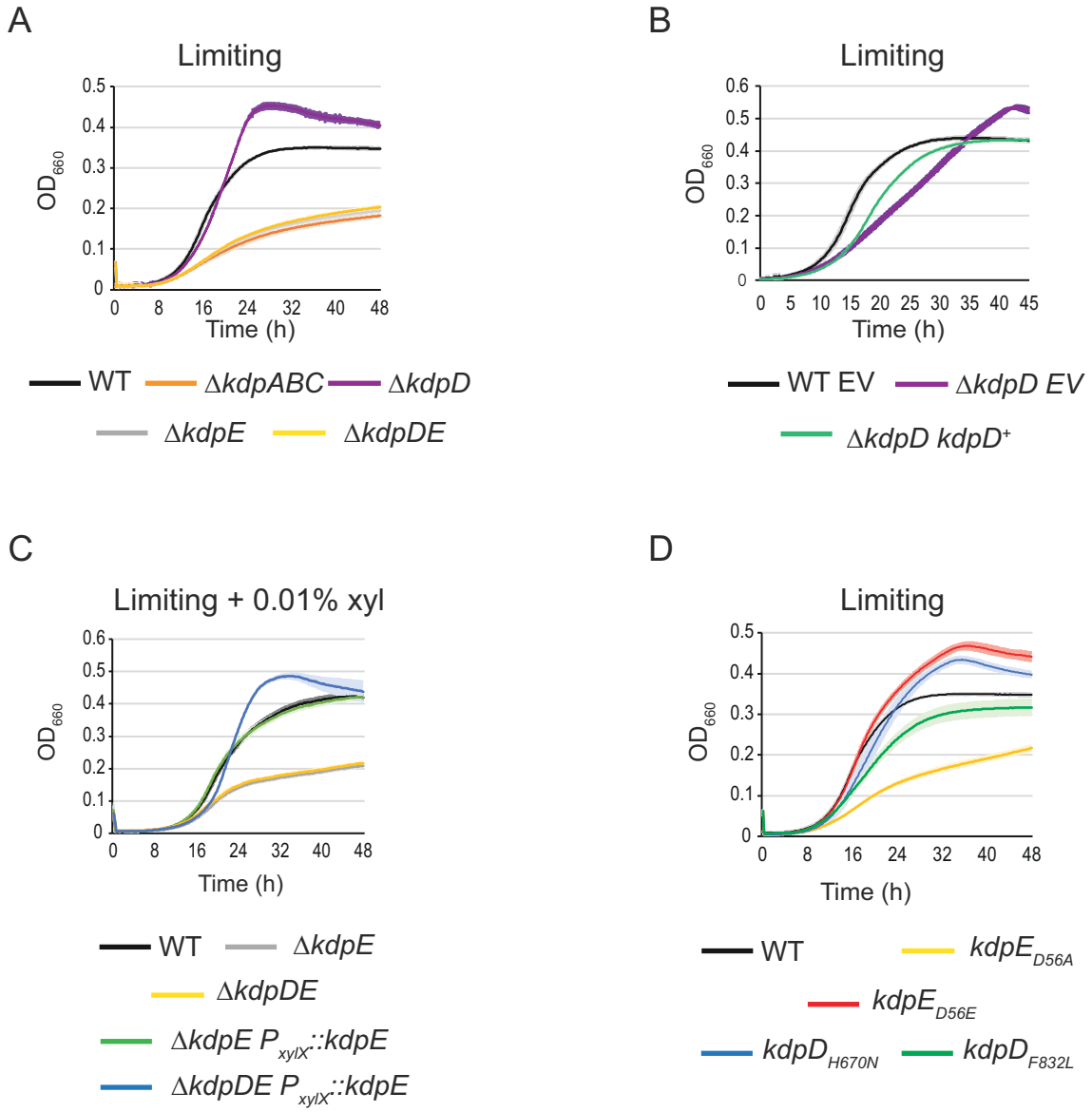

FIG 7 KdpD downregulates KdpE to control growth in low K^+. (A) Growth of WT, Δ*kdpABC*, Δ*kdpD*, Δ*kdpE*, and Δ*kdpDE*. (B) Growth of WT and Δ*kdpD* carrying either pMR10 empty vector (EV) or pMR10 P_{kdp}::*kdpD*. (C) Growth of WT, Δ*kdpE*, and Δ*kdpDE* expressing *kdpE* from the *xylX* locus (P_{xylX}::*kdpE*). (D) Growth of *kdpD* and *kdpE* catalytic point mutants. Growth was done in minimal medium M2G-K supplemented with limiting (0.025 mM) K^+ concentrations (A–D), and tetracycline for plasmid selection (B) or with 0.01% xylose for the induction of *kdpE* expression (C). Data represent average, $n = 3$, and error bars = ±SD.

As expected, a KdpD catalytically dead mutant ($kdpD_{H670N}$) phenocopied Δ*kdpD* in limited K^+ (Fig. 7D; Fig. S5F). Since $kdpE_{D56A}$ cells had a much stronger growth delay than Δ*kdpD* or $kdpD_{H670N}$, it indicates that KdpE is still phosphorylated despite the absence of KdpD. Thus, KdpE is very likely phosphorylated by another—non-cognate—HK. On the other hand, the fact that $kdpE_{D56E}$ cells grew slightly but reproducibly better than Δ*kdpD* and $kdpD_{H670N}$ suggests that KdpD also phosphorylates KdpE, at least during the early exponential phase of growth. Thus, KdpD might (i) phosphorylate KdpE in early exponential phase, with at least another HK, and (ii) mainly act as a phosphatase on KdpE~P in late exponential phase, likely to downregulate the expression of *kdp* and restrict growth in K^+-limiting conditions (Fig. S5G).

To test this hypothesis, we constructed a KdpD kinase-deficient but phosphatase active mutant (K^-/P^+) by replacing a conserved phenylalanine residue by a leucine residue

(*kdpD*$_{F832L}$) in the F box involved in ATP binding, in a way reminiscent to what was described for another HK encoding gene, *pleC*$_{F778L}$ (49) (Fig. S5D). Interestingly, we found that unlike the *kdpD*$_{H670N}$, *kdpD*$_{F832L}$ cells failed to reach a higher plateau in stationary phase (Fig. 7D; Fig. S5F), strongly supporting our hypothesis that KdpD primarily works as a phosphatase in late exponential phase. Moreover, the K^-/P^+ mutant *kdpD*$_{F832L}$ grew better than *kdpE*$_{D56A}$ and Δ*kdpE* mutants in low K^+ conditions (Fig. 7D; Fig. S5F), supporting that there is indeed at least another HK that phosphorylates KdpE. Finally, the fact that the *kdpD*$_{F832L}$ mutant had a growth delay compared to WT suggests that KdpD also acts as a kinase for KdpE in early exponential phase (Fig. 7D; Fig. S5F). However, we cannot rule out the possibility that the phosphatase activity of KdpD$_{F832L}$ is impacted by the mutation. For instance, it might be stronger than the WT, thereby interfering with the phosphorylation levels of KdpE in early exponential phase. Nevertheless, our results altogether indicate that (i) KdpD works both as a kinase and a phosphatase to control KdpE phosphorylation (KdpE~P) levels depending on the growth phase and K^+ availability and that (ii) KdpE can be phosphorylated by (an)other non-cognate HK(s) for regulating K^+ transport in K^+-depleted environments.

KdpD-dependent regulation of the *kdp* promoter in low K^+ conditions

In order to study the Kdp system at the transcriptional level, a plasmid carrying a P*$_{kdp}$::lacZ* reporter fusion was introduced in the different mutant strains, cells were grown in limiting or abundant K^+ conditions and β-galactosidase activity was measured. Consistent with the idea that the Kdp system is a high-affinity potassium transporter, P*$_{kdp}$* basal activity in WT cells was barely detectable at abundant K^+ concentration while it was strongly induced in WT (normalized to 100%) or even more in Δ*kdpABC* cells upon K^+ depletion (Fig. 8A). In contrast, P*$_{kdp}$* activity was completely annihilated in Δ*kdpE* and *kdpE*$_{D56A}$ cells (Fig. 8A), indicating that phosphorylated KdpE (KdpE~P) is strictly required for *kdp* expression both in limiting and abundant K^+ conditions. In support of that, the basal activity of P*$_{kdp}$* was even higher in *kdpE*$_{D56E}$ cells grown at abundant K^+ concentration than in WT cells grown in limiting K^+ conditions (Fig. 8A). In contrast, the histidine kinase KdpD seems not to be required for *kdp* expression at low K^+ concentration since P*$_{kdp}$* was as active in Δ*kdpD* as in WT cells starved for K^+ and still active in *kdpD*$_{H670N}$ or *kdpD*$_{F832L}$ cells (Fig. 8A). However, when the hydrolase activity of KdpD was inactivated, that is in Δ*kdpD* or *kdpD*$_{H670N}$ cells, the basal P*$_{kdp}$* activity at abundant K^+ concentration was, on average, higher than in WT or *kdpD*$_{F832L}$, although these differences were not significant (Fig. 8A). Together, these results suggest that KdpD mainly works as a phosphatase on KdpE~P independently of K^+ availability.

To further characterize the role of KdpD in the regulation of *kdp* expression, we measured the activity of the P*$_{kdp}$::lacZ* fusion in WT and *kdpD* mutant cells along the growth at limiting K^+ concentration. First, the activity of P*$_{kdp}$* in Δ*kdpD* cells was slightly lower than the WT during early exponential phase but higher in stationary phase (Fig. 8B, compare the yellow to the orange bars at 20–24 h and 48 h). On the contrary, *kdp* expression was significantly lower both in *kdpD*$_{H670N}$ (K^-/P^-) and in *kdpD*$_{F832L}$ (K^-/P^+) during early exponential phase, but increased when reaching the late exponential only in *kdpD*$_{H670N}$ cells (Fig. 8B, compare the blue to the brown bars at 20–24 h and 48 h).

Altogether, these results support our hypothesis that (i) KdpD mainly works as a phosphatase and that (ii) KdpE is mainly phosphorylated by another non-cognate kinase.

DISCUSSION

As the most abundant monovalent cation used by living cells to drive many cellular processes, regulating K^+ homeostasis is critical for survival. The oligotrophic α-proteobacterium *C. crescentus* is cyclically subjected to nutrients deprivation in its natural environments. Here, we characterized the response of *C. crescentus* depending on K^+ availability. First, we determined the range of K^+ concentrations at which *C. crescentus* supports growth. Then, we identified all the genes predicted to code for proteins involved in transport, sensing, and regulation of K^+ homeostasis. In addition, we defined

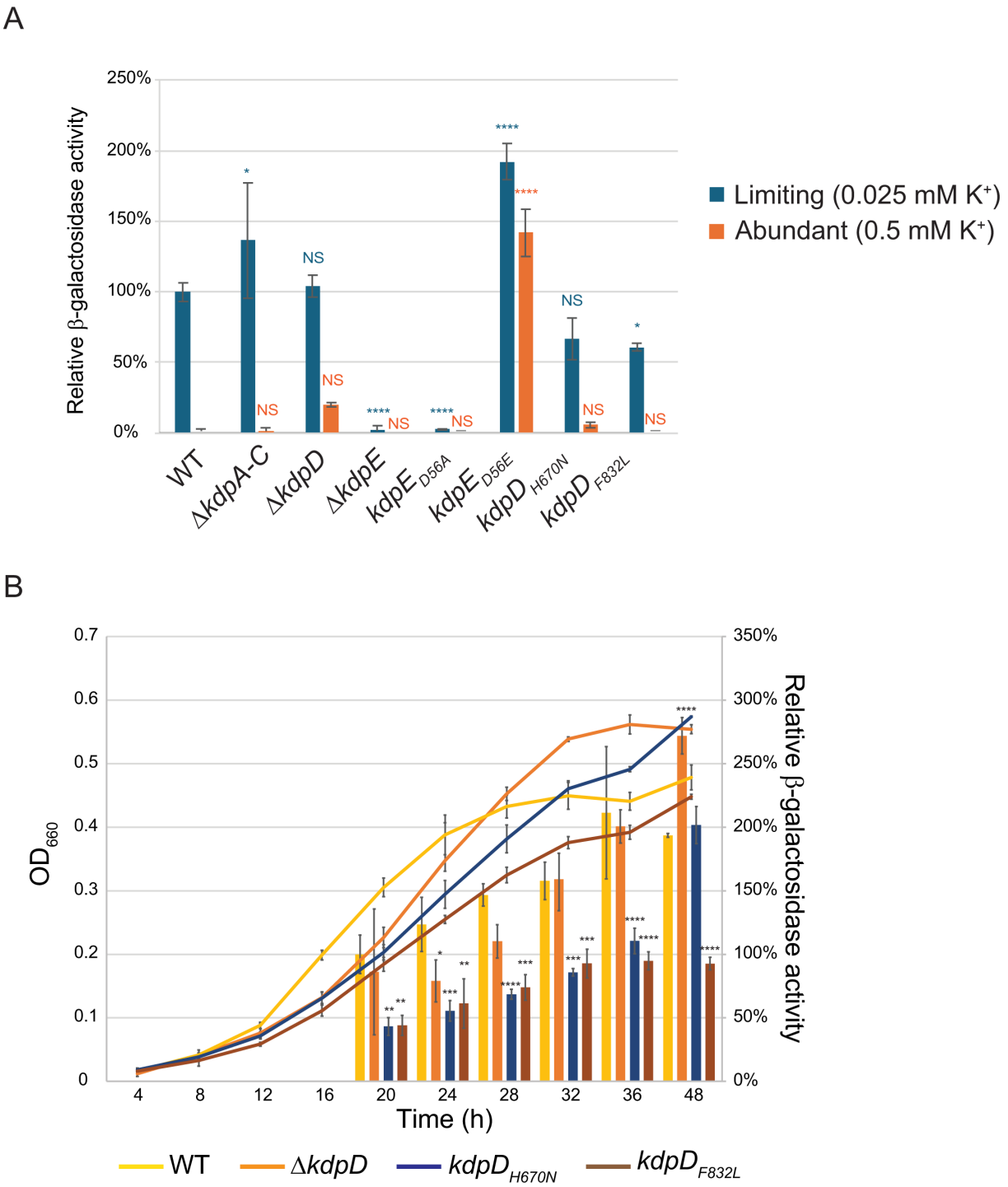

FIG 8 Regulation of *kdp* expression. (A) Relative β-galactosidase activities of WT and *kdp* mutants carrying a transcriptional P_{kdp}::*lacZ* fusion grown in M2G-K supplemented with limiting (0.025 mM) or abundant (0.5 mM) K^+ concentrations. The data were normalized to the WT grown in limiting K^+ conditions (blue bars). (B) Relative β-galactosidase activities of WT and *kdp* mutants carrying a transcriptional P_{kdp}::*lacZ* fusion along the growth in M2G-K supplemented with limiting (0.025 mM). The data were normalized to the WT grown in limiting K^+ conditions (orange bars) after 20 h of growth. Data represent average, $n = 3$, and error bars = ±SD. Means were statistically compared using a two-way analysis of variance, followed by Tukey's multiple comparisons test; not significant (NS), $P < 0.05$ (*), $P < 0.01$ (**), $P < 0.001$ (***), $P < 0.0001$ (****).

the set of genes (i) becoming essential and/or (ii) being induced upon K^+ depletion. This allowed us to find that the low-affinity and the high-affinity K^+ transporters, respectively,

Kup and KdpABC, are critical components that maintain K^+ homeostasis in *C. crescentus*. Finally, we dissected the role played by the TCS regulatory system KdpDE in the response to K^+ depletion.

By analyzing the Tn-seq data, we found that the biological functions for which the highest number of genes that became essential or HFC upon K^+ limitation (M2G vs M2G-K) were (i) C "energy production and conversion" (~1% increase of essential and ~6% increase of HFC) and (ii) J "Translation, ribosomal structure and biogenesis" (~2% increase of essential and ~3% increase of HFC). In fact, it is not so surprising these two categories are sensitive to K^+ availability since ATP concentration and respiration state are two well-known parameters that drive K^+ transport across the membrane. For instance, the electron transport chain determines the membrane potential, which in turn will influence the distribution of other ions like K^+ that accumulate on the cytoplasmic face of the membrane. This might therefore explain why Tn insertions in genes coding for subunits of the respiratory chain or the ATP synthase are counter-selected when K^+ became limiting. On top of this, active transport of K^+ across the membrane by Kdp consumes a large amount of ATP, so decreasing ATP concentration might likely have a negative impact on K^+ import. On the other hand, K^+ cations are critical for maintaining the structure and sustaining the ribosomal functions. Not only is K^+ required to stabilize the transfer RNAs (tRNAs), the ribosomal RNAs (rRNAs), and proteins within the ribosomes, but also to increase proofreading by accommodating the right aminoacyl-tRNA in the ribosomal A-site (50, 51). Additionally, many GTPases involved in translation display a K^+-dependent activation of GTP hydrolysis (1). Thus, the impact K^+ has on translation could explain the lower density of Tn insertion observed in tRNAs and ribosomal genes in cells grown in limiting K^+ conditions.

KdpDE is the major bacterial system described in the literature to respond to limiting K^+ availability. The K^+-dependent regulon of *C. crescentus* allowed us to identify almost 600 genes whose expression changes upon K^+ limitation. Surprisingly, only a small proportion of this regulon depends directly or indirectly on the response regulator KdpE, suggesting that there are unknown transcriptional regulators sensitive to K^+ availability. Based on our Tn-seq data, genes coding for transcriptional regulators that became essential in K^+-limiting conditions might constitute good candidates for such a function (Table S2).

Although KdpE is mainly described to regulate the expression of the *kdp* genes, a few studies already suggested it might control other cellular processes. For instance in *E. coli*, 197 differentially expressed genes with an FC ≥1.5 were identified in a *kdpE* knock-out mutant vs WT grown in K^+-limiting conditions (0.1 mM KCl). These genes are involved in transport and metabolism of carbohydrates and nucleotides, energy production, and conversion (52). ChIP-seq experiments performed in the plant pathogen *Lonsdalea quercina* subsp. *populi* revealed that KdpE interacts with 44 promoter regions of genes related to cell morphology and division, transcription and translation, and nucleotide and carbohydrate metabolism (53).

The analysis of the *C. crescentus* genome allowed us to identify several systems predicted to transport K^+. By systematically characterizing the growth profile of the corresponding mutants in different K^+ regimes, we found that the high-affinity Kdp system primarily serves to import K^+ at limiting concentrations, like in many other bacterial species. Nonetheless, Kdp is unlikely the sole K^+ transport system involved in this context since, despite a growth defect, the Δ*kdpABC* mutant was still able to grow at low K^+ concentration. Interestingly, we found that the low-affinity Kup transporter became dispensable in such limiting K^+ conditions. However, suppressor mutations in Kup (A87P, G253S, and S456R) that improved the growth the Δ*kdp* mutant at low K^+ concentration, without impacting the growth when K^+ was abundant, were selected. A plausible explanation would be that mutations found in Kup increase its affinity for K^+, thereby increasing K^+ transport to compensate the loss of Kdp. In support of that, MD simulations have revealed structural changes in the putative K^+ binding cavity of Kup. First, all the mutants led to the flipping of E263 to a position closer to the one

described for the corresponding E233 in KimA when bound to K^+, which likely makes the second binding pocket accessible and would allow the coordination of another K^+ cation. Indeed, the position observed for E263 in the modeled WT Kup configuration appears to interfere with the second K^+ binding site. Second, the carboxylate group of D146 was made more available for K^+ coordination within this second binding site in a way similar to the one described for the corresponding D117 in KimA. Third, compared to the WT Kup, positions of Y61 and Y410 in the G253S and S456R mutants were also found to be shifted toward the positions observed for the corresponding Y43 and Y377 in KimA, thereby exposing to a greater extent their tyrosyl moiety toward the inside of the cavity where K^+ ion is located. Such structural modifications would be induced by local reorganization of H bonds at the mutation sites, resulting in a cascade of subtle conformational changes toward the binding cavity. While the introduction of P87 abrogates two potential H bonds between A87 and the backbone of V83 and V84, S253 can form new H bonds with an adjacent α-helix, thanks to its polar side chain (Fig. S3B and C). Conversely, mutation of S456 into R456 decreases the number of intra-helix H bonds through the loss of the hydroxyl moiety (Fig. S3D). The available Cryo-EM structure of KimA likely represents an inward-occluded state in which two K^+ cations are trapped in the intracellular cavity by the ideally positioned Y43, D117, E233, and Y377 residues (48). Thus, our *in silico* results are consistent with a higher K^+ affinity observed experimentally in Kup mutants, likely due to the reorientation of the corresponding Y61, D146, E263, and Y410 residues into a "KimA bound to K^+"-like configuration, which consequently enhances K^+ coordination.

Beside Kup, other unknown transporters could participate to K^+ uptake in such limiting conditions. Several putative transporters were identified as essential and HFC in our Tn-seq analysis (*CCNA_01159*) and upregulated in the RNA-seq analysis (*CCNA_00339*, *CCNA_01852*, *CCNA_01587*, *CCNA_01588*, *CCNA_02570*, *CCNA_02571*). It is possible that one or several of them second the activity of KdpABC in limiting K^+ conditions.

As in *E. coli*, the expression of *kdp* operon in *C. crescentus* is activated upon K^+ starvation by the KdpDE TCS (54). However, we found surprising differences since in the absence of the HK KdpD, (i) *kdp* is still expressed and (ii) the *kdp* promoter (P_{kdp}) is more active in the stationary phase. Our genetic dissection of the catalytic activity of KdpDE with point mutants in *kdpE* (phospho-mimetic $kdpE_{D56E}$ and phospho-ablative $kdpE_{D56A}$) and KdpD (K^-/P^- $kdpD_{H670N}$ and K^-/P^+ $kdpD_{F832L}$) strongly suggests that (i) KdpE is phosphorylated by another—non-cognate—HK and that (ii) KdpD works mainly as a phosphatase.

In *E. coli*, deletion of the *kdpD* results in a prominent growth arrest of more than 20 h, before restarting growth thanks to KdpE phosphorylation by PhoR. However, it never surpassed the WT plateau as seen with *C. crescentus* Δ*kdpD*, $kdpD_{H670N}$, and $kdpE_{D56E}$ mutants. Thus, the higher plateau is likely due to the loss of KdpD phosphatase activity. The phosphatase activity of KdpD has been shown in *E. coli* to be stimulated by intracellular K^+ levels (23). Four amino acids located in the second periplasmic loop were identified as an extracellular K^+-specific recognition site. In contrast, the K^+ recognition site for intracellular sensing remains to be identified. However, although specific residues could not be highlighted, the C-terminal cytoplasmic domain of KdpD was described to display a K^+-dependent phosphatase activity (20, 55). Authors suggested that the cytoplasmic GAF domain of KdpD may be responsible for intracellular K^+ sensing. Most GAF domains are involved in regulatory functions through binding to cyclic nucleotides or other small ligands including ions (55, 56). However, *C. crescentus* KdpD lacks a GAF domain, which suggests that such a connection between intracellular sensing and phosphatase activity does not exist in *C. crescentus* (Fig. S5D). Recently, it was reported that *E. coli* KdpD also works as serine kinase in high K^+ concentrations to control KdpB ATPase activity and ultimately stop Kdp-dependent K^+ transport (57). The phosphorylated serine residue in KdpB as well as the two Walker (A and B) domains in tandem driving the serine kinase activity of KdpD are conserved in *C. crescentus* (Fig. S6), indicating that this post-transcriptional control of K^+ influx might also work in *C. crescentus*.

As mentioned above, in *E. coli*, the sensor kinase PhoR can crosstalk with KdpE, which allows a Δ*kdpD* mutant to grow in a low K^+ environment after a long lag phase (21). Since PhoR is conserved in *C. crescentus*, it constitutes a good candidate for the non-cognate HK phosphorylating KdpE, although based on our Tn-seq data, the *phoR* gene seems dispensable on low K^+ plates (Table S2).

The nitrogen-related phosphotransferase component $EIIA^{Ntr}$ has been shown in *E. coli* to regulate K^+ transport by modulating KdpD kinase activity (26, 58, 59). For instance, in limiting K^+ conditions (<5 mM), the unphosphorylated form of $EIIA^{Ntr}$ was shown to directly interact with KdpD and stimulate its kinase activity, thereby promoting phosphorylation of KdpE and the subsequent increase of *kdp* genes expression (25). This $EIIA^{Ntr}$-based control of KdpD has also been reported in the plant symbionts *Rhizobium leguminosarum* (60) and *Sinorhizobium fredii* (8), two α-proteobacteria closely related to *C. crescentus*. It was later discovered that $EIIA^{Ntr}$ regulates σ factor selectivity by modulating K^+ levels. Indeed, the competition between σ^{70} and σ^S for interaction with the RNA polymerase (RNAP) is influenced by K^+ intracellular levels (61). Depending on the phosphorylation state of $EIIA^{Ntr}$, the resulting K^+ intracellular levels preferentially favor the binding of either σ^{70} or σ^S to the core RNAP (61). Interestingly, PTS^{Ntr} components regulate the levels of another signaling molecule—(p)ppGpp—that connects cell division with environmental and metabolic cues in *C. crescentus* (62–64). Knowing that (p)ppGpp also influences gene expression by regulating σ factor competition (65), it is therefore tempting to speculate that $EIIA^{Ntr}$ and/or (p)ppGpp participate to the K^+ homeostasis in *C. crescentus*, even in other α-proteobacteria.

MATERIALS AND METHODS

Bacterial strains and growth conditions

All *Escherichia coli* strains used in this thesis were grown aerobically in Luria-Bertani (LB) broth (Sigma). *E. coli* Top10 was used for cloning purpose, while *E. coli* MT607 was used for tri-parental matings. Thermo-competent cells were used for transformation of *E. coli*. All *Caulobacter crescentus* strains used are derived from the synchronizable wild-type strain NA1000. The traditional synthetic medium supplemented with glucose (M2G) was modified by replacing potassium salts by their equivalent sodium salts to obtain a medium without any K^+ (K_0) to which the desired K^+ concentrations could be added. The source of K^+ consists in both KH_2PO_4 and K_2HPO_4 mixed to an equivalent ratio in terms of K^+ concentration. For each experiment, cells were first grown at 30°C; in PYE, then adapted overnight at 30°C in K_0 medium supplemented with 0.5 mM K^+, washed twice in K_0 medium, and finally grown at 30°C in K_0 medium supplemented with the desired K^+ concentration. For growth curve measurements, cultures were diluted to a final OD_{660} of 0.02 in a 96-well plate. Growth was monitored during 48 h with continuous shaking at 30°C, in an automated plate reader (Bioscreen C, Lab Systems) measuring OD_{660} every 10 min. For *E. coli*, antibiotics were used at the following concentrations (µg/mL; in liquid/solid medium): chloramphenicol (20/30), kanamycin (30/50), oxytetracycline (12.5/12.5), spectinomycin (100/100), and streptomycin (50/100), while for *C. crescentus*, media were supplemented with kanamycin (5/20), oxytetracycline (2.5/2.5), and nalidixic acid (20) when appropriate. Genes under the control of the inducible xylose promoter (P_{xylX}) were induced with 0.1% xylose. Plasmid delivery into *C. crescentus* was achieved by either bi- or tri-parental mating using *E. coli* S17-1 and *E. coli* MT607 as helper strains, respectively. In-frame deletions were created by using the pNPTS138-derivative plasmids as follows. Integration of the plasmids in the *C. crescentus* genome after single homologous recombination was selected on PYE plates supplemented with kanamycin. Three independent recombinant clones were inoculated in PYE medium without kanamycin and incubated overnight at 30°C. Then, dilutions were spread on PYE plates supplemented with 3% sucrose and incubated at 30°C (except for *kup* deletion as specified in the Results section). Single colonies were picked and transferred onto PYE plates with and without kanamycin. Finally, to discriminate between mutated and wild-type loci,

kanamycin-sensitive clones were tested by PCR on colony using locus-specific oligonucleotides.

Spotting assays

Ten-fold serial dilutions (in M2G-K) were prepared in 96-well plates from 5 mL cultures in standard universal tubes grown overnight at 30°C in the corresponding medium. Cells (5 µL) were then spotted on plates, incubated at 30°C for 2 to 3 days and pictures were taken.

β-Galactosidase assays

β-Galactosidase assays were performed as already described in reference (42). Briefly, cultures were either grown to stationary phase directly in a 96-well plate or grown in flasks from which samples were withdrawn throughout growth and placed at −80°C in between time points. Permeabilization of cells was performed by incubating cells with lysis buffer (20 mg/mL polymyxin B, β-mercaptoethanol) for 30 min at 28°C. Then, 50 µL of 4 mg/mL O-nitrophenyl-β-D-galactopyranoside (ONPG) were added. Lysis and ONPG solutions were prepared using Z buffer as a solvent (60 mM Na_2HPO_4, 40 mM NaH_2PO_4, 10 mM KCl, 1 mM $MgSO_4$, pH 7.0). Both OD_{420} and OD_{550} were measured every minute for 30 min at 30°C using a fluorimeter (SpectraMax, Molecular Devices). Miller units (MU) were calculated using the following formula: $MU = (OD_{420} \times 1{,}000) / [OD_{660} \times t \times v]$ where t is the reaction time in min, and v is the volume of culture used in milliliters. Then, ONPG hydrolysis was measured at 30°C for 30 min. The activity of the β-galactosidase expressed in MU was calculated using the following equation: $MU = (OD_{420} \times 1{,}000) / [OD_{660} \times t \times v]$ where t is the time of the reaction (min), and v is the volume of cultures used in the assays (mL). Experimental values were the average of three independent experiments.

Protein purification and production of polyclonal antibodies

To immunize rabbits for production of polyclonal antibodies, an *E. coli* BL21 (DE3) pLysS strain carrying plasmid pET-28a-*kdpE* was grown in LB medium supplemented with kanamycin and chloramphenicol until an OD_{600} of 0.5. After addition of Isopropyl-β-D-thiogalactopyranoside (IPTG) to a final concentration of 1 mM, the culture was incubated at 18°C for 18 h. Cells were then harvested by centrifugation for 30 min at 5,000 × *g*, at 4°C. The pellet was resuspended in 20 mL of binding buffer (20 mM Tris-HCl pH 8.0, 500 mM NaCl, 10% glycerol, 10 mM $MgCl_2$, 12.5 mM imidazole) supplemented with complete EDTA-free protease cocktail inhibitor (Roche), 400 mg lysozyme (Sigma), and 10 mg DNaseI (Roche), and incubated for 30 min on ice. Cells were then lysed by sonication. After centrifugation at 12,000 rpm for 30 min at 4°C, the lysate was loaded on a Ni-NTA column and incubated for 1 h at 4°C with end-over-end agitation. The column was then washed with 5 mL binding buffer, 3 mL Wash1 buffer (binding buffer with 25 mM imidazole), 3 mL Wash2 buffer (binding buffer with 50 mM imidazole), and 3 mL Wash3 buffer (binding buffer with 75 mM imidazole). Proteins bound to the column were eluted with 3 mL elution buffer (binding buffer with 100 mM imidazole) and aliquoted in 300 µL fractions. All the fractions containing the protein of interest (checked by Coomassie blue staining) were pooled and dialyzed in dialysis buffer (20 mM Tris pH 8, 500 mM NaCl, 10% glycerol). Purified KdpE was used to immunize rabbits (CER Groupe, Marloie, Belgium).

Tn-seq analysis

A mini-Tn5 was introduced in *C. crescentus* NA1000 WT strain by bi-parental mating. Briefly, overnight cultures of recipient and donor strains (grown in LB supplemented with kanamycin) were mixed in 95:5 ratio to a final volume of 1 mL. Cells were harvested by centrifugation at 9,000 rpm (7,600 × *g*) at room temperature (RT) for 2 min. The

supernatant was removed, and 1 mL of fresh PYE medium was added to wash the pellet. A second centrifugation step was done to remove again the supernatant. Thereafter, the pellet was resuspended in 50 µL and spotted on PYE agar and incubated at 30°C for 4 h. Cells were collected, resuspended in 10 mL M2G or M2G-K, and washed twice with the same volume. Dilutions (10^{-6}) were plated on M2G or M2G-K plates supplemented with aztreonam (5 µg mL^{-1}) and kanamycin (5 µg mL^{-1}) and incubated at 30°C for 5 days. Then, at least 3×10^5 colonies were collected in M2G or M2G-K supplemented with 10% glycerol and stored at −80°C. Genomic DNA was then extracted following the Nucleospin Tissue Kit protocol (Macherey-Nagel) and resuspended in 50 µL elution buffer (5 mM Tris-HCl [pH 8.5]). DNA sequencing was performed using an Illumina NextSeq (paired-end 2 × 75) instrument (Fasteris, Geneva, Switzerland). Reads corresponding to the mini-Tn5 insertion sites were first filtered with the 5′-GGTTGAGATGTGT ATAAGAGACAG sequence before being processed as described in reference (66). Briefly, filtered reads were mapped on the genome of *C. crescentus* NA1000 (GenBank accession number NC_011916.1) and converted to Sequence Alignment/Map (SAM) format using the Burrows-Wheeler Aligner and SAMtools, respectively, from the Sourceforge server (https://sourceforge.net/). Next, the number of reads overlapping each genomic position was computed using custom Python scripts. The total number of reads for internal 80% of each Open Reading Frame (ORF) in each condition was then computed using custom Python scripts. For comparing strains, the total number of reads was normalized by the ratio of the number of reads between the two strains. Ward's clustering analysis was performed to define the fitness categories as previously reported (41), which are (i) essential, (ii) HFC, and (iii) non-essential. The number of clusters was arbitrarily set to 10 with ORFs from cluster 1 classified as essential, from cluster 2 as high fitness cost, and those from clusters 3–10 as non-essential.

For the M2G library, genes with values of Tn insertions / bp ≤ 0.01333333 were considered as essential, 0.01333779 ≤ and ≤ 0.04063018 as HFC, and ≥ 0.04081632 as non-essential. For the M2G-K library, genes values of ≤ 0.0047112 were considered as essential, 0.0047909 ≤ and ≤ 0.0211178 as HFC, and ≥ 0.0215792 as non-essential.

Chromatin immunoprecipitation followed by deep sequencing (ChIP-seq assay)

ChIP-seq was performed as already described in reference (66). Briefly, 80 mL of mid-log-phase cells (OD_{660} of 0.6) was cross-linked in 1% formaldehyde and 10 mM sodium phosphate (pH 7.6) at RT for 10 min and then for 30 min on ice. Cross-linking was stopped by addition of 125 mM glycine and incubated for 5 min on ice. Cells were washed twice in phosphate buffer solution (137 mM NaCl, 2.7 mM KCl, 10 mM Na_2HPO_4, 1.8 mM KH_2PO_4, pH 7.4), resuspended in 450 µL TES buffer [10 mM Tris-HCl (pH 7.5), 1 mM EDTA, and 100 mM NaCl], and lysed with 2 µL of Ready-Lyse lysozyme solution for 5 min at RT. Protease inhibitors (Roche) were added, and the mixture was incubated for 10 min. Then, 550 µL of ChIP buffer [1.1% Triton X-100, 1.2 mM EDTA, 16.7 mM Tris-HCl (pH 8.1), 167 mM NaCl, protease inhibitors] was added to the lysate and incubated at 37°C for 10 min before sonication (2 × 8 bursts of 30 s on ice using a Diagenode Bioruptor) to shear DNA fragments to a length of 300 to 500 bp. Lysate was cleared by centrifugation for 10 min at 12,500 rpm at 4°C, and protein content was assessed by measuring the OD_{280}. Then, 7.5 mg of proteins was diluted in ChIP buffer supplemented with 0.01% SDS and precleared for 1 h at 4°C with 50 µL of SureBeads Protein A Magnetic Beads (BioRad) and 100 µg bovine serum albumin (BSA). One microliter of polyclonal anti-KdpE antibodies was added to the supernatant before overnight incubation at 4°C under gentle agitation. Next, 80 µL of BSA presaturated protein A-agarose beads was added to the solution and incubated for 2 h at 4°C with rotation, washed once with low-salt buffer [0.1% SDS, 1% Triton X-100, 2 mM EDTA, 20 mM Tris-HCl (pH 8.1), 150 mM NaCl], once with high-salt buffer [0.1% SDS, 1% Triton X-100, 2 mM EDTA, 20 mM Tris-HCl (pH 8.1), 500 mM NaCl], once with LiCl buffer [0.25 M LiCl, 1% NP-40, 1% deoxycholate, 1 mM EDTA, 10 mM Tris-HCl (pH 8.1)], and once with TE buffer [10 mM Tris-HCl (pH 8.1)

1 mM EDTA] at 4°C, followed by a second wash with TE buffer at RT. The DNA-protein complexes were eluted twice in 250 µL freshly prepared elution buffer (0.1 M NaHCO3, 1% SDS). NaCl was added at a concentration of 300 mM to the combined eluates (500 µL) before overnight incubation at 65°C to reverse the cross-link. The samples were treated with 20 µg of proteinase K in 40 mM EDTA and 40 mM Tris-HCl (pH 6.5) for 2 h at 45°C. DNA was extracted using a Nucleospin PCR cleanup kit (Macherey-Nagel) and resuspended in 50 µL elution buffer [5 mM Tris-HCl (pH 8.5)]. DNA sequencing was performed using an Illumina NextSeq 550 (paired-end 2 × 75 or 2 × 100) instrument (Seqalis). Next Generation Sequencing (NGS) data were analyzed as described in reference (66).

RNA-seq

WT and Δ*kdpE* cells were grown overnight to OD_{660} ~0.3 in M2G-K 0,025 mM K^+ and WT in M2G-K 0,5 mM K^+. Thereafter, total RNA was extracted with RNeasy Protect Bacteria Kit from Qiagen and following manufacturer's instructions. The quantity and quality (A260/A280 ration) of RNA was determined with a Thermo Scientific Nanodrop One Microvolume UV-Vis Spectrophotometer. RNA-seq TTRNA libraries were prepared from total RNA after ribodepletion with the Illumina Ribo-Zero Plus rRNA Depletion kit and sequenced with Illumina NovaSeq 6000 (paired-end 2 × 100) instrument (Seqalis). NGS data were analyzed using Galaxy (https://usegalaxy.org) (42). Briefly, FastQC was used to evaluate the quality of the reads; HISAT2 was used to map the reads onto the NA1000 reference genome (NC_011916.1) and generate bam files; featureCounts was used to generate counts tables using bam files; and DESeq2 was used to determine differentially expressed genes. The volcano plot was generated using GraphPad Prism 9 software.

Statistical analyses

All the statistical analyses were performed using GraphPad Prism 9 software. A *P*-value of <0.05 was considered as significant.

Molecular dynamics simulations

Protein systems were prepared for simulations from the three-dimensional model of Kup from *Caulobacter crescentus* (UniProt ID: Q9ABT9 or B8GXM1) generated with AlphaFold2 (67). A87P, G253S, and S456R mutants were manually edited from the WT structure at the corresponding position via the PyMOL software (version 2.5.2). As the putative potassium binding site of Kup is located within its transmembrane helixes, the N-terminal (residues 1 to 38) and C-terminal (residues 499 to 665) domains were truncated to reduce computational costs. The resulting structural models (WT, A87P, G253S, and S456R) were properly protonated at pH 7.5 via the ProteinPrepare tool implemented in PlayMolecule (68). The CHARMMGUI suite was used for building the lipid bilayer, the insertion of Kup, and for the generation of input files using the Membrane Builder interface (69, 70). Based on the reported composition of *Caulobacter* inner membrane, a mix of 90% 1,2-dioleoyl-sn-glycero-3-phosphoglycerol (DOPG) and 10% tetraoleoyl cardiolipin (TOCL2) was selected to better reflect the native environment of Kup (46, 47). Each protein structure was oriented along the z-axis, perpendicular to the lipid bilayer, with the transmembrane helix constituted from residue R77 to M104. The upper leaflet contained 65 DOPG and 7 TOCL2 molecules, whereas the lower leaflet was composed of 63 and 7 DOPG and TOCL2 molecules, respectively. KUP-embedded lipidic systems were solvated in TIP3P water, neutralized with K^+ cations, and supplemented with 150 mM KCl. All-atom MD simulations were carried out with the GROMACS 2023.1 suite package (71) on Kup WT, A87P, G253S, and S456R systems, using CHARMM36m force field (72). Overall calculation efficiency was improved by hydrogen mass repartitioning (HMR), allowing to increase the time step to 4 fs. The energy of each system was first minimized within 5,000 steps using the steepest descent method. Systems were further equilibrated successively at a temperature of 300 K and a pressure of 1 bar by the use of Berendsen thermostat and barostat, respectively, for a total of 1,875 ps. Production MD were performed at 300

K and 1 bar with the Nosé-Hoover thermostat and the Parinello-Rahman barostat for 1 µs each. Long-range electrostatic interactions were taken into account by means of the particle mesh Ewald (PME) summation. Periodic boundary conditions (PBCs) were set in all three dimensions, and atom trajectories were recorded every 4 ps. The final frame of each run was extracted and visualized with the PyMOL software (version 2.5.2). The latter was also used to create the presented snapshots and figures.

ACKNOWLEDGMENTS

We thank the members of the Hallez lab for critical reading of the manuscript and helpful discussions. The authors are also appreciative to the PTCI high-performance computing resource of the University of Namur. The present research benefited from computational resources made available on Lucia, the Tier-1 supercomputer of the Walloon Region, infrastructure funded by the Walloon Region under the grant agreement no. 1910247.

This work was supported by the Fonds de la Recherche Scientifique – FNRS (F.R.S. – FNRS) with a Welbio Starting Grant (WELBIO-CR-2019S-05) to R.H. A.Q.-Y. was supported by a postdoctoral fellowship from the University of Namur (UNamur). L.L. and J.M. are both supported by the F.R.S. – FNRS, as a postdoctoral researcher for L.L. and a research fellow for J.M. C.M and R.H. are senior research associates of the F.R.S. – FNRS.

AUTHOR AFFILIATIONS

[1]Bacterial Cell cycle & Development (BCcD), Biology of Microorganisms Research Unit (URBM), Namur Research Institute for Life Science (NARILIS), Universite de Namur, Namur, Belgium
[2]Laboratoire de Chimie Physique des Biomolécules, UCPTS, Namur Institute of Structured Matter (NISM), Namur Research Institute for Life Sciences (NARILIS), Universite de Namur, Namur, Belgium
[3]WEL Research Institute, University of Namur, Namur, Belgium

AUTHOR ORCIDs

Alex Quintero-Yanes http://orcid.org/0000-0002-8350-0881
Régis Hallez http://orcid.org/0000-0003-1175-8565

FUNDING

Funder	Grant(s)	Author(s)
Walloon excellence in life sciences and biotechnology (WELBIO)	WELBIO-CR-2019S-05	Régis Hallez
AUL | Université de Namur (UNamur)	FSR Postdoctoral Fellowship	Quintero-Yanes Alex
Waalse Gewest (Walloon Region)	1910247	Catherine Michaux

AUTHOR CONTRIBUTIONS

Alex Quintero-Yanes, Conceptualization, Data curation, Formal analysis, Investigation, Methodology, Validation, Visualization, Writing – original draft | Loïc Léger, Data curation, Formal analysis, Investigation, Methodology, Validation, Visualization | Madeline Collignon, Data curation, Formal analysis, Investigation, Methodology, Validation, Visualization | Julien Mignon, Data curation, Formal analysis, Investigation, Methodology, Validation, Visualization | Aurélie Mayard, Formal analysis, Methodology, Visualization | Catherine Michaux, Conceptualization, Data curation, Methodology, Resources, Validation, Visualization | Régis Hallez, Conceptualization, Data curation, Funding acquisition, Methodology, Project administration, Resources, Supervision, Validation, Visualization, Writing – original draft, Writing – review and editing

DATA AVAILABILITY

ChIP-seq, RNA-seq, and Tn-seq data have been deposited to the Gene Expression Omnibus (GEO) repository with the accession numbers GSE253227, GSE253228, and GSE253229.

ADDITIONAL FILES

The following material is available online.

Supplemental Material

Supplemental figures (JB00107-24-s0001.pdf). Figures S1 to S6.
Supplemental tables and methods (JB00107-24-s0002.pdf). Tables S1 and S2; construction of plasmids.
Table S3 (JB00107-24-s0003.xlsx). RNA_Seq WT in abundant (0.5 mM) and limiting (0.025 mM) K+.
Table S4 (JB00107-24-s0004.xlsx). RNA_Seq WT and ΔkdpE in limiting (0.025 mM) K+.

REFERENCES

1. Danchin A, Nikel PI. 2019. Why nature chose potassium. J Mol Evol 87:271–288. https://doi.org/10.1007/s00239-019-09915-2
2. Epstein W. 2003. The roles and regulation of potassium in bacteria. Prog Nucleic Acid Res Mol Biol 75:293–320. https://doi.org/10.1016/s0079-6603(03)75008-9
3. Bakker EP, Mangerich WE. 1981. Interconversion of components of the bacterial proton motive force by electrogenic potassium transport. J Bacteriol 147:820–826. https://doi.org/10.1128/jb.147.3.820-826.1981
4. Booth IR. 1999. The regulation of intracellular pH in bacteria. Novartis Found Symp 221:19–28. https://doi.org/10.1002/9780470515631.ch3
5. Ochrombel I, Ott L, Krämer R, Burkovski A, Marin K. 2011. Impact of improved potassium accumulation on pH homeostasis, membrane potential adjustment and survival of *Corynebacterium glutamicum*. Biochim Biophys Acta 1807:444–450. https://doi.org/10.1016/j.bbabio.2011.01.008
6. Castañeda-García A, Do TT, Blázquez J. 2011. The K^+ uptake regulator TrkA controls membrane potential, pH homeostasis and multidrug susceptibility in *Mycobacterium smegmatis*. J Antimicrob Chemother 66:1489–1498. https://doi.org/10.1093/jac/dkr165
7. Domínguez-Ferreras A, Muñoz S, Olivares J, Soto MJ, Sanjuán J. 2009. Role of potassium uptake systems in *Sinorhizobium meliloti* osmoadaptation and symbiotic performance. J Bacteriol 191:2133–2143. https://doi.org/10.1128/JB.01567-08
8. Feng XY, Tian Y, Cui WJ, Li YZ, Wang D, Liu Y, Jiao J, Chen WX, Tian CF. 2022. The PTS^{Ntr}-KdpDE-KdpFABC pathway contributes to low potassium stress adaptation and competitive nodulation of *Sinorhizobium fredii*. mBio 13:e0372121. https://doi.org/10.1128/mbio.03721-21
9. Gries CM, Bose JL, Nuxoll AS, Fey PD, Bayles KW. 2013. The Ktr potassium transport system in *Staphylococcus aureus* and its role in cell physiology, antimicrobial resistance and pathogenesis. Mol Microbiol 89:760–773. https://doi.org/10.1111/mmi.12312
10. Humphries J, Xiong L, Liu J, Prindle A, Yuan F, Arjes HA, Tsimring L, Süel GM. 2017. Species-independent attraction to biofilms through electrical signaling. Cell 168:200–209. https://doi.org/10.1016/j.cell.2016.12.014
11. Liu Y, Ho KK, Su J, Gong H, Chang AC, Lu S. 2013. Potassium transport of *Salmonella* is important for type III secretion and pathogenesis. Microbiology (Reading) 159:1705–1719. https://doi.org/10.1099/mic.0.068700-0
12. MacGilvary NJ, Kevorkian YL, Tan S. 2019. Potassium response and homeostasis in *Mycobacterium tuberculosis* modulates environmental adaptation and is important for host colonization. PLoS Pathog 15:e1007591. https://doi.org/10.1371/journal.ppat.1007591
13. Prindle A, Liu J, Asally M, Ly S, Garcia-Ojalvo J, Süel GM. 2015. Ion channels enable electrical communication in bacterial communities. Nature 527:59–63. https://doi.org/10.1038/nature15709
14. Quintero-Yanes A, Monson RE, Salmond GPC. 2019. Environmental potassium regulates bacterial flotation, antibiotic production and turgor pressure in *Serratia* through the TrkH transporter. Environ Microbiol 21:2499–2510. https://doi.org/10.1111/1462-2920.14637
15. Rasmussen T. 2023. The potassium efflux system Kef: bacterial protection against toxic electrophilic compounds. Membranes (Basel) 13:465. https://doi.org/10.3390/membranes13050465
16. Su J, Gong H, Lai J, Main A, Lu S. 2009. The potassium transporter Trk and external potassium modulate *Salmonella enterica* protein secretion and virulence. Infect Immun 77:667–675. https://doi.org/10.1128/IAI.01027-08
17. Valente RS, Xavier KB. 2016. The Trk potassium transporter is required for RsmB-mediated activation of virulence in the phytopathogen *Pectobacterium wasabiae*. J Bacteriol 198:248–255. https://doi.org/10.1128/JB.00569-15
18. Pedersen BP, Stokes DL, Apell HJ. 2019. The KdpFABC complex - K^+ transport against all odds. Mol Membr Biol 35:21–38. https://doi.org/10.1080/09687688.2019.1638977
19. Ali MK, Li X, Tang Q, Liu X, Chen F, Xiao J, Ali M, Chou SH, He J. 2017. Regulation of inducible potassium transporter KdpFABC by the KdpD/KdpE two-component system in *Mycobacterium smegmatis* Front Microbiol 8:570. https://doi.org/10.3389/fmicb.2017.00570
20. Dani P, Ujaoney AK, Apte SK, Basu B. 2017. Regulation of potassium dependent ATPase (kdp) operon of *Deinococcus radiodurans*. PLoS One 12:e0188998. https://doi.org/10.1371/journal.pone.0188998
21. Schramke H, Laermann V, Tegetmeyer HE, Brachmann A, Jung K, Altendorf K. 2017. Revisiting regulation of potassium homeostasis in *Escherichia coli*: the connection to phosphate limitation. Microbiologyopen 6:e00438. https://doi.org/10.1002/mbo3.438
22. Laermann V, Ćudić E, Kipschull K, Zimmann P, Altendorf K. 2013. The sensor kinase KdpD of *Escherichia coli* senses external K^+. Mol Microbiol 88:1194–1204. https://doi.org/10.1111/mmi.12251
23. Schramke H, Tostevin F, Heermann R, Gerland U, Jung K. 2016. A dual-sensing receptor confers robust cellular homeostasis. Cell Rep 16:213–221. https://doi.org/10.1016/j.celrep.2016.05.081
24. Heermann R, Weber A, Mayer B, Ott M, Hauser E, Gabriel G, Pirch T, Jung K. 2009. The universal stress protein UspC scaffolds the KdpD/KdpE signaling cascade of *Escherichia coli* under salt stress. J Mol Biol 386:134–148. https://doi.org/10.1016/j.jmb.2008.12.007
25. Lüttmann D, Heermann R, Zimmer B, Hillmann A, Rampp IS, Jung K, Görke B. 2009. Stimulation of the potassium sensor KdpD kinase activity by interaction with the phosphotransferase protein IIA(Ntr) in *Escherichia coli*. Mol Microbiol 72:978–994. https://doi.org/10.1111/j.1365-2958.2009.06704.x
26. Mörk-Mörkenstein M, Heermann R, Göpel Y, Jung K, Görke B. 2017. Non-canonical activation of histidine kinase KdpD by phosphotransferase

protein PtsN through interaction with the transmitter domain. Mol Microbiol 106:54–73. https://doi.org/10.1111/mmi.13751
27. Bossemeyer D, Borchard A, Dosch DC, Helmer GC, Epstein W, Booth IR, Bakker EP. 1989. K+-transport protein TrkA of *Escherichia coli* is a peripheral membrane protein that requires other trk gene products for attachment to the cytoplasmic membrane. J Biol Chem 264:16403–16410.
28. Dosch DC, Helmer GL, Sutton SH, Salvacion FF, Epstein W. 1991. Genetic analysis of potassium transport loci in *Escherichia coli*: evidence for three constitutive systems mediating uptake potassium. J Bacteriol 173:687–696. https://doi.org/10.1128/jb.173.2.687-696.1991
29. Harms C, Domoto Y, Celik C, Rahe E, Stumpe S, Schmid R, Nakamura T, Bakker EP. 2001. Identification of the ABC protein SapD as the subunit that confers ATP dependence to the K+-uptake systems Trk(H) and Trk(G) from *Escherichia coli* K-12. Microbiology (Reading) 147:2991–3003. https://doi.org/10.1099/00221287-147-11-2991
30. Schleyer M, Bakker EP. 1993. Nucleotide sequence and 3'-end deletion studies indicate that the K+ -uptake protein kup from *Escherichia coli* is composed of a hydrophobic core linked to a large and partially essential hydrophilic C terminus. J Bacteriol 175:6925–6931. https://doi.org/10.1128/jb.175.21.6925-6931.1993
31. Zakharyan E, Trchounian A. 2001. K+ influx by Kup in *Escherichia coli* is accompanied by a decrease in H+ efflux. FEMS Microbiol Lett 204:61–64. https://doi.org/10.1111/j.1574-6968.2001.tb10863.x
32. Hartl J, Kiefer P, Kaczmarczyk A, Mittelviefhaus M, Meyer F, Vonderach T, Hattendorf B, Jenal U, Vorholt JA. 2020. Untargeted metabolomics links glutathione to bacterial cell cycle progression. Nat Metab 2:153–166. https://doi.org/10.1038/s42255-019-0166-0
33. Skerker JM, Laub MT. 2004. Cell-cycle progression and the generation of asymmetry in *Caulobacter crescentus*. Nat Rev Microbiol 2:325–337. https://doi.org/10.1038/nrmicro864
34. Beaufay F, Coppine J, Hallez R. 2021. When the metabolism meets the cell cycle in bacteria. Curr Opin Microbiol 60:104–113. https://doi.org/10.1016/j.mib.2021.02.006
35. Bossemeyer D, Schlösser A, Bakker EP. 1989. Specific cesium transport via the *Escherichia coli* Kup (TrkD) K+ uptake system. J Bacteriol 171:2219–2221. https://doi.org/10.1128/jb.171.4.2219-2221.1989
36. Cao Y, Jin X, Huang H, Derebe MG, Levin EJ, Kabaleeswaran V, Pan Y, Punta M, Love J, Weng J, Quick M, Ye S, Kloss B, Bruni R, Martinez-Hackert E, Hendrickson WA, Rost B, Javitch JA, Rajashankar KR, Jiang Y, Zhou M. 2011. Crystal structure of a potassium ion transporter, TrkH. Nature 471:336–340. https://doi.org/10.1038/nature09731
37. Roosild TP, Castronovo S, Healy J, Miller S, Pliotas C, Rasmussen T, Bartlett W, Conway SJ, Booth IR. 2010. Mechanism of ligand-gated potassium efflux in bacterial pathogens. Proc Natl Acad Sci U S A 107:19784–19789. https://doi.org/10.1073/pnas.1012716107
38. Heermann R, Jung K. 2010. The complexity of the 'simple' two-component system KdpD/KdpE in *Escherichia coli*. FEMS Microbiol Lett 304:97–106. https://doi.org/10.1111/j.1574-6968.2010.01906.x
39. Roe AJ, McLaggan D, O'Byrne CP, Booth IR. 2000. Rapid inactivation of the *Escherichia coli* Kdp K+ uptake system by high potassium concentrations. Mol Microbiol 35:1235–1243. https://doi.org/10.1046/j.1365-2958.2000.01793.x
40. Laimins LA, Rhoads DB, Epstein W. 1981. Osmotic control of kdp operon expression in *Escherichia coli*. Proc Natl Acad Sci U S A 78:464–468. https://doi.org/10.1073/pnas.78.1.464
41. Curtis PD, Brun YV. 2014. Identification of essential alphaproteobacterial genes reveals operational variability in conserved developmental and cell cycle systems. Mol Microbiol 93:713–735. https://doi.org/10.1111/mmi.12686
42. Quintero-Yanes A, Mayard A, Hallez R. 2022. The two-component system ChvGI maintains cell envelope homeostasis in *Caulobacter crescentus*. PLoS Genet 18:e1010465. https://doi.org/10.1371/journal.pgen.1010465
43. de Oliveira MVV, Intorne AC, Vespoli L de S, Andrade LF, Pereira L de M, Rangel PL, de Souza Filho GA. 2017. Essential role of K+ uptake permease (Kup) for resistance to sucrose-induced stress in *Gluconacetobacter diazotrophicus* PAl 5. Environ Microbiol Rep 9:85–90. https://doi.org/10.1111/1758-2229.12503
44. Trchounian A, Kobayashi H. 1999. Kup is the major K+ uptake system in *Escherichia coli* upon hyper-osmotic stress at a low pH. FEBS Lett 447:144–148. https://doi.org/10.1016/s0014-5793(99)00288-4
45. Hocking J, Priyadarshini R, Takacs CN, Costa T, Dye NA, Shapiro L, Vollmer W, Jacobs-Wagner C. 2012. Osmolality-dependent relocation of penicillin-binding protein PBP2 to the division site in *Caulobacter crescentus*. J Bacteriol 194:3116–3127. https://doi.org/10.1128/JB.00260-12
46. Chow TC, Schmidt JM. 1974. Fatty acid composition of *Caulobacter crescentus*. Microbiology 83:369–373. https://doi.org/10.1099/00221287-83-2-369
47. Contreras I, Shapiro L, Henry S. 1978. Membrane phospholipid composition of *Caulobacter crescentus*. J Bacteriol 135:1130–1136. https://doi.org/10.1128/jb.135.3.1130-1136.1978
48. Tascón I, Sousa JS, Corey RA, Mills DJ, Griwatz D, Aumüller N, Mikusevic V, Stansfeld PJ, Vonck J, Hänelt I. 2020. Structural basis of proton-coupled potassium transport in the KUP family. Nat Commun 11:626. https://doi.org/10.1038/s41467-020-14441-7
49. Matroule JY, Lam H, Burnette DT, Jacobs-Wagner C. 2004. Cytokinesis monitoring during development; rapid pole-to-pole shuttling of a signaling protein by localized kinase and phosphatase in *Caulobacter*. Cell 118:579–590. https://doi.org/10.1016/j.cell.2004.08.019
50. Grason JP, Gresham JS, Widjaja L, Wehri SC, Lorimer GH. 2008. Setting the chaperonin timer: the effects of K+ and substrate protein on ATP hydrolysis. Proc Natl Acad Sci U S A 105:17334–17338. https://doi.org/10.1073/pnas.0807429105
51. Rozov A, Khusainov I, El Omari K, Duman R, Mykhaylyk V, Yusupov M, Westhof E, Wagner A, Yusupova G. 2019. Importance of potassium ions for ribosome structure and function revealed by long-wavelength X-ray diffraction. Nat Commun 10:2519. https://doi.org/10.1038/s41467-019-10409-4
52. Choudhary KS, Kleinmanns JA, Decker K, Sastry AV, Gao Y, Szubin R, Seif Y, Palsson BO. 2020. Elucidation of regulatory modes for five two-component systems in *Escherichia coli* reveals novel relationships. mSystems 5. https://doi.org/10.1128/mSystems.00980-20
53. Yang RL, Deng CY, Wei JW, He W, Li AN, Qian W. 2018. A large-scale mutational analysis of two-component signaling systems of *Lonsdalea quercina* revealed that KdpD-KdpE regulates bacterial virulence against host poplar trees. Mol Plant Microbe Interact 31:724–736. https://doi.org/10.1094/MPMI-10-17-0248-R
54. Polarek JW, Williams G, Epstein W. 1992. The products of the kdpDE operon are required for expression of the Kdp ATPase of *Escherichia coli*. J Bacteriol 174:2145–2151. https://doi.org/10.1128/jb.174.7.2145-2151.1992
55. Cann M. 2007. A subset of GAF domains are evolutionarily conserved sodium sensors. Mol Microbiol 64:461–472. https://doi.org/10.1111/j.1365-2958.2007.05669.x
56. Heikaus CC, Pandit J, Klevit RE. 2009. Cyclic nucleotide binding GAF domains from phosphodiesterases: structural and mechanistic insights. Structure 17:1551–1557. https://doi.org/10.1016/j.str.2009.07.019
57. Silberberg JM, Ketter S, Böhm PJ, Jordan K, Wittenberg M, Grass J, Hänelt I. 2023. Sensory kinase KdpD is a tandem serine histidine kinase controlling K+ump KdpFABC on the translational and post-transcriptional level. bioRxiv. https://doi.org/10.1101/2023.11.09.566405:2023.11.09.566405
58. Lüttmann D, Göpel Y, Görke B. 2015. Cross-talk between the canonical and the nitrogen-related phosphotransferase systems modulates synthesis of the KdpFABC potassium transporter in *Escherichia coli*. J Mol Microbiol Biotechnol 25:168–177. https://doi.org/10.1159/000375497
59. Zimmer B, Hillmann A, Görke B. 2008. Requirements for the phosphorylation of the *Escherichia coli* EIIANtr protein *in vivo*. FEMS Microbiol Lett 286:96–102. https://doi.org/10.1111/j.1574-6968.2008.01262.x
60. Untiet V, Karunakaran R, Krämer M, Poole P, Priefer U, Prell J. 2013. ABC transport is inactivated by the PTS(Ntr) under potassium limitation in *Rhizobium leguminosarum* 3841. PLoS One 8:e64682. https://doi.org/10.1371/journal.pone.0064682
61. Lee CR, Cho SH, Kim HJ, Kim M, Peterkofsky A, Seok YJ. 2010. Potassium mediates *Escherichia coli* enzyme IIA(Ntr) -dependent regulation of sigma factor selectivity. Mol Microbiol 78:1468–1483. https://doi.org/10.1111/j.1365-2958.2010.07419.x
62. Hallez R, Delaby M, Sanselicio S, Viollier PH. 2017. Hit the right spots: cell cycle control by phosphorylated guanosines in alphaproteobacteria. Nat Rev Microbiol 15:137–148. https://doi.org/10.1038/nrmicro.2016.183

63. Ronneau S, Petit K, De Bolle X, Hallez R. 2016. Phosphotransferase-dependent accumulation of (p)ppGpp in response to glutamine deprivation in *Caulobacter crescentus*. Nat Commun 7:11423. https://doi.org/10.1038/ncomms11423
64. Shyp V, Dubey BN, Böhm R, Hartl J, Nesper J, Vorholt JA, Hiller S, Schirmer T, Jenal U. 2021. Reciprocal growth control by competitive binding of nucleotide second messengers to a metabolic switch in *Caulobacter crescentus*. Nat Microbiol 6:59–72. https://doi.org/10.1038/s41564-020-00809-4
65. Jishage M, Kvint K, Shingler V, Nyström T. 2002. Regulation of sigma factor competition by the alarmone ppGpp. Genes Dev 16:1260–1270. https://doi.org/10.1101/gad.227902
66. Coppine J, Kaczmarczyk A, Petit K, Brochier T, Jenal U, Hallez R. 2020. Regulation of bacterial cell cycle progression by redundant phosphatases. J Bacteriol 202:e00345-20. https://doi.org/10.1128/JB.00345-20
67. Jumper J, Evans R, Pritzel A, Green T, Figurnov M, Ronneberger O, Tunyasuvunakool K, Bates R, Žídek A, Potapenko A, et al. 2021. Highly accurate protein structure prediction with AlphaFold. Nature 596:583–589. https://doi.org/10.1038/s41586-021-03819-2
68. Martínez-Rosell G, Giorgino T, De Fabritiis G. 2017. PlayMolecule ProteinPrepare: a web application for protein preparation for molecular dynamics simulations. J Chem Inf Model 57:1511–1516. https://doi.org/10.1021/acs.jcim.7b00190
69. Jo S, Kim T, Iyer VG, Im W. 2008. CHARMM-GUI: a web-based graphical user interface for CHARMM. J Comput Chem 29:1859–1865. https://doi.org/10.1002/jcc.20945
70. Park S, Choi YK, Kim S, Lee J, Im W. 2021. CHARMM-GUI membrane builder for lipid nanoparticles with Ionizable cationic lipids and PEGylated lipids. J Chem Inf Model 61:5192–5202. https://doi.org/10.1021/acs.jcim.1c00770
71. Abraham MJ, Murtola T, Schulz R, Páll S, Smith JC, Hess B, Lindahl E. 2015. GROMACS: high performance molecular simulations through multi-level parallelism from laptops to supercomputers. SoftwareX 1–2:19–25. https://doi.org/10.1016/j.softx.2015.06.001
72. Huang J, Rauscher S, Nawrocki G, Ran T, Feig M, de Groot BL, Grubmüller H, MacKerell AD Jr. 2017. CHARMM36m: an improved force field for folded and intrinsically disordered proteins. Nat Methods 14:71–73. https://doi.org/10.1038/nmeth.4067